1970

An investigation of the stiffness of shafts with integral disks

Richard King Riley

AN INVESTIGATION OF THE STIFFNESS OF SHAFTS WITH INTEGRAL DISKS

BY

RICHARD KING RILEY, 1936 -

A

DISSERTATION

submitted to the faculty of

THE UNIVERSITY OF MISSOURI - ROLLA

in partial fulfillment of the requirements for the

Degree of

DOCTOR OF PHILOSOPHY IN MECHANICAL ENGINEERING

Rolla, Missouri

1970

Approved by

J. R. Fawcett (advisor) Peter G. Hansen

Wm. J. Gatley Glen Haddock

Harold Dean Keith Jerry F. Lehnhoff

ABSTRACT

The results of an investigation of the effect of an integral disk on the torsional elastic stiffness of an axisymmetric shaft are presented. Various configurations of disk diameters and widths on a shaft of specified diameter were investigated, using a finite element method of calculation verified by experimentation. The finite element method is presented for the elastic solution of a general axisymmetric body under all possible axisymmetric load conditions. The axisymmetric body is idealized as an assemblage of triangular cross-sectioned torii representing both the normal and shear properties. The elastic stiffness is used to obtain the equilibrium equations of the assemblage, which are solved for displacements of the structure. The experimental work included the design of the torsional testing apparatus, specimens, and the experimental technique. The results indicate the effectiveness of an integral disk in resisting torsional deflection for the various shaft configurations. An approximate method of finding the stiffness of disks for aluminum shafts is also presented.

PREFACE

Accurate prediction of the deflections of structures under load is of vital design significance. Recently developed high strength materials have allowed designers to reduce the size of load carrying members to a point where in many cases, deflections and vibrational characteristics dictate the design limit rather than stress levels. Only with accurate stiffness or flexibility information can design criteria such as natural frequencies and interference distances be satisfied. The problem of torque carrying shafts has long been an area of concern to engineers, but the interest has been in finding the stress state rather than deflections. This is particularly true for work on shafts with abrupt diameter changes, where the efforts have been directed toward finding the stress state in the transition fillet.

This presentation is devoted to an evaluation of the flexibility of a shaft with one or more integral disks, which introduce abrupt diameter changes in close proximity. Included in the presentation are two approaches to the problem; a numerical technique usable for calculating the displacement field of any axisymmetric solid, and an experimental apparatus usable for accurate twist measurements.

ACKNOWLEDGEMENTS

The author wishes to thank his supervising professor, Dr. Thomas R. Faucett, for patience, guidance, and assistance throughout the course of this work. The assistance, advice, and encouragement of Dr. Harold D. Keith on the finite element methods is gratefully acknowledged.

In addition, the author would like to thank Dr. A. G. Haddock, Dr. P. G. Hansen, Dr. W. S. Gatley, and Dr. T. F. Lehnhoff for serving on his thesis committee. No acknowledgement could be complete without a mention of the support and encouragement of his wife and family.

TABLE OF CONTENTS

Appendix

LIST OF ILLUSTRATIONS

LIST OF TABLES

NOMENCLATURE AND LIST OF SYMBOLS

The following symbols are used in this presentation. The prime (') indicates a quantity associated with the local coordinate system.

*,**	- footnote symbol
$[\ ]$	- matrix of dimensions r X s
$\{\ \}$	- column matrix(vector)
$[\ ]^T$	- transpose of a matrix
$[\ ]^{-1}$	- inverse of a square matrix
e	- superscript denoting a quantity associated with a particular element
r, θ, z	- global coordinates
r', θ', z'	- local coordinates
r_i, θ_i, z_i	- global coordinates of a spatial point indicated by i
r_i', θ_i', z_i'	- local coordinates of a spatial point indicated by i
u, v, w	- generalized global displacements
u', v', w'	- generalized local displacements
u_i, v_i, w_i	- generalized global displacements of a spatial point indicated by i
$\{f\}$	- generalized displacement vector in global coordinates
$\{f'\}$	- generalized displacement vector in local coordinates
$\{\alpha\}$	- vector of constants for displacement expansion of an element
$[P]$	- displacement expansion coordinate matrix for spatial point

$[P_i]$ - displacement expansion coordinate matrix for the i-th node

$[\tilde{P}]$ - generalized displacement expansion coordinate matrix for one displacement of a spatial point

$[\tilde{P}_i]$ - generalized displacement expansion coordinate matrix for one displacement of the i-th node

$\{\delta\}$ - nodal displacement vector

$\{\delta_i\}$ - nodal displacement vector for the i-th node

$\{\delta'\}$ - nodal displacement vector in local coordinates

δ_i - element of nodal displacement vector

$[C]$ - matrix of global coordinate parameters for an element

$[\tilde{C}]$ - matrix of global coordinate parameters in a displacement direction

$[C']$ - matrix of local coordinate parameters for an element

C_{ij} - element of the inverse coordinate matrix

$[N]$ - generalized displacement field matrix of an element

$\epsilon_r, \epsilon_\theta, \epsilon_z$ - normal engineering strains

$\gamma_{r\theta}, \gamma_{rz}, \gamma_{\theta z}$ - shear engineering strains

$[\tilde{0}]$ - 1 X 6 null vector

$\{\epsilon\}$ - strain field vector of an element

$\{\epsilon_o\}$ - initial strain field vector of an element

$[G]$ - strain-displacement field matrix of an element

$[B]$ - strain interpolation matrix of an element

σ_r, σ_θ, σ_z	- normal engineering stresses
$\sigma_{r\theta}$, σ_{rz}, $\sigma_{\theta z}$	- shearing engineering stresses
$\{\sigma\}$	- stress field vector of an element
E	- modulus of elasticity
ν	- Poisson's ratio
G	- shearing modulus of elasticity
λ_1, λ_2	- elastic constants
V	- volume of an element
A	- cross-sectional area of a ring element
$[D]$	- elasticity matrix of an element
$[K]$	- global stiffness matrix
$[\tilde{K}]$	- global stiffness submatrix
k_{ij}	- element of the global stiffness matrix
$\{F\}_{\epsilon_o}$	- element load vector due to initial strains
$\{F\}_p$	- element load vector due to body forces
$\{F\}_s$	- element load vector due to surface forces
$\{F\}_r$	- element load vector due to node loads
a_i, b_i, c_i	- initial strain interpolation constants
$\{p\}$	- body force matrix
ρ	- material density
ω	- angular velocity
A_z	- longitudinal acceleration
$\{S\}$	- surface load vector

d_i	- surface load interpolation constants
β	- angle of element boundary to 'r' axis
s	- distance along a surface
S	- generator of the exterior boundary of an element
$\{R_i\}$	- concentrated load vector on the i-th node
$\{Q\}$	- load matrix for assembled structure
$[L]$	- reduced stiffness matrix
l_{ij}	- element of reduced stiffness matrix
$\{Y\}$	- substitution load vector
y_i	- element of substitution load vector
ϕ	- angle of twist
T	- applied torque
J	- polar moment of inertia
Z	- generator of boundary over a length of a shaft
$[T]$	- transformation matrix
$[\tilde{T}]$	- transformation submatrix
I	- area integral
η_1, η_2	- line boundary constants

CHAPTER I

INTRODUCTION

The original interest in torsional load carrying shafts with abrupt changes of diameters arose from the need to know the maximum stress in a filletted shaft, and indeed much interest is still shown in this important problem. The work in this area has progressed along several avenues since the general mathematical equations for torsion in a solid of revolution were defined. The classical equations are well known and are found in most elasticity texts(1-3).* Because of the importance of a knowledge of stress levels for design, the efforts of investigators have been directed toward this end.

The first significant work on the solution of the equations was done by Willers(4), who used a graphical integration technique to obtain the solution for stepped and collared shafts. Approximate analytical solutions were found for given shapes of stepped shafts by Sonntag (5), which give an evaluation of the surface stresses. A continuation of the process for solving the equations implicitly has led to a solution for some other special geometries(6-7), but these are quite limited.

---

*Numbers underlined and in parentheses refer to listings in the Bibliography.

As the interest in the area grew, several experimental techniques were found to evaluate these stresses, including both analogic experimental solutions and direct evaluation. Usable electrical analogs of the torsional stress problem were found by Jacobson(8) in terms of electrical potential, and a less difficult method was utilized by Thum and Bautz(9) to evaluate stresses in various shapes. Both methods have difficulties in providing a practical complete analogy, which limits their general use. Experimental determinations of the stress concentrations for various shapes were found by Wiegand (10), and these results agree with the values of Sonntag (5). These values are in common use and have appeared in many English language books, subh as that by Peterson (11). With the introduction of three-dimensional photoelastic materials and the accompanying experimental techniques required, it was shown by Frocht(12) that this method was applicable to finding stress states due to torsion in solids of revolution.

The use of numerical techniques for the solution of shafts in torsion was begun with the work of Thom and Orr(13). They applied the finite difference procedure to obtain solutions for surface stresses of stepped and collared shafts. The use of finite difference techniques has continued to be developed and improved. Later formulations are given by Southwell(14).

The finite element displacement method for linear structures and solids is now well established. Since the work of Turner, et al.(15), the effort in this area has been considerable. Several texts(16-17) furnish extensive references to this work. A number of finite element programs are available for use on two-dimensional problems. One is given by Zienkiewicz(17) and others are available through government agencies, such as Sass II(18). Several programs are also available for complete three-dimensional structures and solids. No programs are currently available which treat the axisymmetric body when it is loaded in torsion, except the complete three-dimensional programs which require considerably more computational effort to use than is necessary.

Little attention has been devoted to the problem of the deflection of the variable diameter shaft. Some solutions of deflections of these geometries are available, by Timoshenko(3), but only for smooth shapes. The techniques for their solution are about the same as those for the stresses, but they have not been applied.

This presentation is devoted to evaluation of the stiffness of integral disks on shafts. The two abrupt diameter changes in close proximity give a drastic variation from a smooth geometry and have considerable effect on the stiffness. The present available evaluation of this deflection is that of the cylindrical shaft in torsion

which does not take into account the diameter changes. It is apparent from the stress levels in a stepped shaft that some of the material in the disk portion is lightly loaded and contributes little to the stiffness.

The means of analysis implemented is to use the finite element method to evaluate the displacements. This method is used rather than either the analytical or the finite difference approach for several reasons. An analytical approach would require the solution of a non-linear boundary value problem. With difficulties found by others in the solutions for stepped shafts, the solution for a shaft with disk is indeed formidable. The use of finite difference techniques would require either a very fine grid or a number of grid size transitions, thus requiring considerable computational effort. A finite element method is developed herein for this general shaft geometry, and provides not only for solutions of this geometry, but also provides a general formulation for axisymmetric solids.

CHAPTER II

REVIEW OF FINITE ELEMENT CONCEPTS

The finite element concept views a continuous structure or body as an assemblage of structural "elements" or subregions which are interconnected at a discrete number of points or nodes. A true continuum would require an infinite number of nodes, but an approximate model is possible with a limited number of nodes. Enforced on each element is a restricted displacement field which is a linear combination of preselected displacement patterns or "shape functions", which are functions of the generalized coordinates. Thus, the displacements of the model are determined from the magnitude of the generalized coordinates associated with the shape functions. The displacement state of the assemblage is determined by minimizing the total potential energy of the assemblage, and this state is then an approximation of the true displacement under a given set of loads.

The accuracy of this method of approximation of structural behavior depends, to a great extent, on the shape function selected, and on the compatibility requirement which is enforced along the boundaries between elements. Certain minimum requirements of these shape functions should be recognized to ensure a close approximation. They are given by Zienkiewicz(17) on page 22 as follows:

(i) The shape functions selected must permit rigid

body displacements without element straining.

(ii) The shape function must provide for the continuity of the displacements thoughout the body of the element and be able to provide continuity between elements.

The procedure used in solving a problem by this method first requires obtaining the stiffness properties of each of the elements in terms of the nodal displacements. By assembling individual elements, the stiffness properties of the complete structure can be obtained. The analysis is completed by the solution of simultaneous nodal point equilibrium equations for nodal displacements.

CHAPTER III

FINITE ELEMENT FORMULATION FOR AXISYMMETRIC ELASTIC SOLIDS

A. THE AXISYMMETRIC CONCEPT

The finite element method used is for a three-dimensional axisymmetric body. This formulation allows for all axisymmetric displacements including displacement due to torsion, which is not included in a two-dimensional type formulation(See Figure 1). Thus, this formulation is an intermediate step between the analysis for two-dimensional type axisymmetric bodies with two allowable displacements such as described by Zienkiewicz(17) in Chapter 4 and a full three-dimensional analysis with three allowable displacements as described by Zienkiewicz(17) in Chapter 6.

The advantages of limiting the formulation to the axisymmetric case of three dimensions are several. First, this allows the elements to be in the form of rings which are triangular cross-sections rotated about the axis of symmetry with node lines rather than points. Using these elements gives several times fewer nodes when the body of interest is discretized. Secondly, when the analysis of the element stiffness characteristic is carried out, the axisymmetric properties allow a much easier analysis.

B. DISPLACEMENT FUNCTIONS

The allowed displacement function or "shape function" which is used is a full quadratic expansion. This "shape function" meets all of the requirements prescribed on

page 5 and ensures that all strains and stresses can take any prescribed linear variation throughout the element.

The displacement variation along the element boundary is then parabolic. Therefore, to ensure continuity of displacement along the boundary, three nodes must be along each side of an element. This formulation was derived by de Veubeke(19) and is also given by Argyris(20).

This gives the element displacement fields as

$$u = \alpha_1 + \alpha_2 r + \alpha_3 z + \alpha_4 r^2 + \alpha_5 rz + \alpha_6 z^2$$

$$v = \alpha_7 + \alpha_8 r + \alpha_9 z + \alpha_{10} r^2 + \alpha_{11} rz + \alpha_{12} z^2 \qquad (3.1)^*$$

$$w = \alpha_{13} + \alpha_{14} r + \alpha_{15} z + \alpha_{16} r^2 + \alpha_{17} rz + \alpha_{18} z^2$$

where the alphas are constant coefficients of the polynomial. The element displacement field can then be written in matrix notation** as

$$\{f^e\} = \begin{Bmatrix} u \\ v \\ w \end{Bmatrix} \qquad (3.2a)$$

---

*Numbers in parentheses refer to equations.

**Matrix notation will be employed throughout this dissertation with symbolic representations defined on page xi.- xiv.

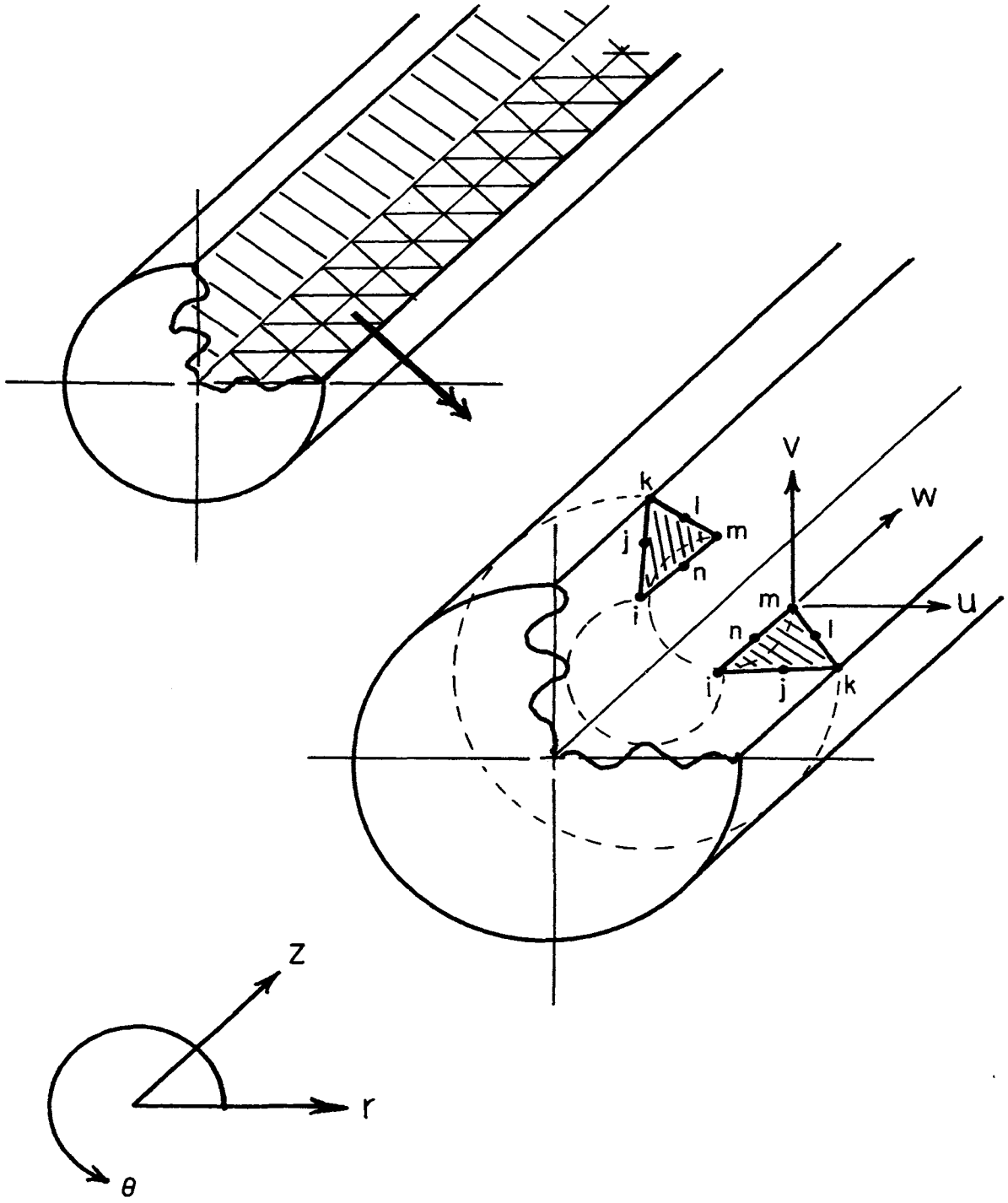

Figure 1. A Typical Finite Element Idealization of an Axisymmetric Solid

or

$$\{f^e\} = [P^e]\begin{Bmatrix} \alpha_1 \\ \alpha_2 \\ \alpha_3 \\ \cdot \\ \cdot \\ \cdot \\ \alpha_{18} \end{Bmatrix} \tag{3.2b}$$

where $[P^e]$ equals

$$\begin{bmatrix} 1 & r & z & r^2 & rz & z^2 & 0 & 0 & 0 & 0 & 0 & 0 & 0 & 0 & 0 & 0 & 0 & 0 \\ 0 & 0 & 0 & 0 & 0 & 0 & 1 & r & z & r^2 & rz & z^2 & 0 & 0 & 0 & 0 & 0 & 0 \\ 0 & 0 & 0 & 0 & 0 & 0 & 0 & 0 & 0 & 0 & 0 & 0 & 1 & r & z & r^2 & rz & z^2 \end{bmatrix} \tag{3.2c}$$

or

$$\{f^e\} = [P^e]\{\alpha^e\} \tag{3.3}$$

The displacement of the i-th node may be expressed as

$$\{\delta_i^e\} = \begin{Bmatrix} u_i \\ v_i \\ w_i \end{Bmatrix} \tag{3.4}$$

and in terms of the coordinate matrix $[P^e]$* evaluated at the global coordinates of the node is

$$\{\delta_i\} = [P]\Big|_{r = r_i,\ z = z_i} \{\alpha\} \tag{3.5}$$

The nodal displacements of all of the nodes of the triangular element can be written as

$$\{\delta\} = \begin{Bmatrix} \delta_1 \\ \delta_2 \\ \delta_3 \\ \cdot \\ \cdot \\ \cdot \\ \delta_6 \end{Bmatrix} \tag{3.6}$$

therefore

$$\{\delta\} = \begin{Bmatrix} P|_1 \\ P|_2 \\ P|_3 \\ \cdot \\ \cdot \\ \cdot \\ P|_6 \end{Bmatrix} \{\alpha\} \tag{3.7}$$

*The superscript ^{e} denoting association with an element will be omitted in the remaining discussion.

where the coordinate matrices $[P]$ are evaluated at the nodal coordinates of the indicated nodes of the element. This can be expressed as

$$\{\delta\} = [C]\{\alpha\} \tag{3.8}$$

The displacement function coefficients may be written as a function of the nodal displacements.

$$\{\alpha\} = [C]^{-1}\{\delta\} \tag{3.9}$$

The element displacement field is written as a function of the nodal displacements of the element.

$$\{f\} = [P][C]^{-1}\{\delta\} \tag{3.10}$$

or in the form

$$\{f\} = [N]\{\delta\} \tag{3.11}$$

where

$$[N] = [P][C]^{-1} \tag{3.11a}$$

The inverse of the nodal coordinate matrix $[C]$ is required. This inversion is evaluated analytically. This inversion is shown in Appendix A.

C. STRAIN-DISPLACEMENT RELATIONS

The element displacement in the cylindrical coordinate system of this formulation is given in Equation (3.10). From this equation, the strains within the

element are then developed in terms of the displacement field coefficients.

The strain-displacement relations for small displacements are given by Boresi(21) on page 248 as

$$\epsilon_r = \frac{\partial u}{\partial r}$$

$$\epsilon_\theta = \frac{u}{r} + \frac{1}{r}\frac{\partial v}{\partial \theta}$$

$$\epsilon_z = \frac{\partial w}{\partial z} \qquad (3.12)$$

$$\gamma_{r\theta} = \frac{1}{r}\frac{\partial u}{\partial \theta} + \frac{\partial v}{\partial r} - \frac{v}{r}$$

$$\gamma_{rz} = \frac{\partial u}{\partial z} + \frac{\partial w}{\partial r}$$

$$\gamma_{\theta z} = \frac{\partial v}{\partial z} + \frac{1}{r}\frac{\partial w}{\partial \theta}$$

In the formulation for the axisymmetric case, the partial derivatives with respect to the angle θ are zero. Therefore the strain displacement relations become

$$\{\epsilon\} = \begin{Bmatrix} \epsilon_r \\ \epsilon_\theta \\ \epsilon_z \\ \gamma_{r\theta} \\ \gamma_{rz} \\ \gamma_{\theta z} \end{Bmatrix} = \begin{Bmatrix} \frac{\partial u}{\partial r} \\ \frac{u}{r} \\ \frac{\partial w}{\partial z} \\ \frac{\partial v}{\partial r} - \frac{v}{r} \\ \frac{\partial u}{\partial z} + \frac{\partial w}{\partial r} \\ \frac{\partial v}{\partial z} \end{Bmatrix} \tag{3.13}$$

The displacement field is defined by Equation (3.2b) and is written in the form

$$\{f\} = \begin{Bmatrix} u \\ v \\ w \end{Bmatrix} = \begin{Bmatrix} \tilde{P} & \tilde{0} & \tilde{0} \\ \tilde{0} & \tilde{P} & \tilde{0} \\ \tilde{0} & \tilde{0} & \tilde{P} \end{Bmatrix} \tag{3.14}$$

where

$$[\tilde{P}] = [1 \quad r \quad z \quad r^2 \quad rz \quad z^2] \tag{3.14a}$$

Therefore the element strains can be defined as

$$\{\epsilon\} = \begin{bmatrix} \frac{\partial \tilde{P}}{\partial r} & \tilde{0} & \tilde{0} \\ \frac{\tilde{P}}{r} & \tilde{0} & \tilde{0} \\ \tilde{0} & \tilde{0} & \frac{\partial \tilde{P}}{\partial z} \\ \tilde{0} & \frac{\partial \tilde{P}}{\partial r} - \frac{\tilde{P}}{r} & \tilde{0} \\ \frac{\partial \tilde{P}}{\partial z} & \tilde{0} & \frac{\partial \tilde{P}}{\partial r} \\ \tilde{0} & \frac{\partial \tilde{P}}{\partial z} & \tilde{0} \end{bmatrix} \{\alpha\} \qquad (3.15)$$

and written as

$$\{\epsilon\} = [G]\{\alpha\} \qquad (3.16)$$

or using Equation (3.9), this becomes

$$\{\epsilon\} = [G][C]^{-1}\{\delta\} \qquad (3.17)$$

The equation is written to define strain in terms of nodal displacements as

$$\{\epsilon\} = [B] \quad \{\delta\} \qquad (3.18)$$

where

$$[B] = [G][C]^{-1} \qquad (3.18a)$$

D. STRESS-STRAIN RELATIONS

The stress-strain relationships for a linearly

elastic isotropic material are given by Timoshenko and Goodier(3) on page 10 as

$$\epsilon_r = \frac{1}{E}(\sigma_r - \nu\sigma_\theta - \nu\sigma_z)$$

$$\epsilon_\theta = \frac{1}{E}(-\nu\sigma_r + \sigma_\theta - \nu\sigma_z)$$

$$\epsilon_z = \frac{1}{E}(-\nu\sigma_r - \nu\sigma_\theta + \sigma_z) \qquad (3.19)$$

$$\gamma_{r\theta} = \frac{1}{G}\sigma_{r\theta}$$

$$\gamma_{rz} = \frac{1}{G}\sigma_{rz}$$

$$\gamma_{\theta z} = \frac{1}{G}\sigma_{\theta z}$$

where E is the modulus of elasticity and ν is Poisson's ratio, and

$$G = \frac{E}{2(1-\nu)} \qquad (3.19a)$$

The desired form of the equation is to have stress as a function of the strain. Also at this point, residual strains allowed in the formulation are entered into the equation. Written in matrix form the strain-stress relations become

$$\{\sigma\} = \begin{Bmatrix} \sigma_r \\ \sigma_\theta \\ \sigma_z \\ \sigma_{r\theta} \\ \sigma_{rz} \\ \sigma_{\theta z} \end{Bmatrix} = \lambda_3 \begin{bmatrix} 1 & \lambda_1 & \lambda_1 & 0 & 0 & 0 \\ \lambda_1 & 1 & \lambda_1 & 0 & 0 & 0 \\ \lambda_1 & \lambda_1 & 1 & 0 & 0 & 0 \\ 0 & 0 & 0 & \lambda_2 & 0 & 0 \\ 0 & 0 & 0 & 0 & \lambda_2 & 0 \\ 0 & 0 & 0 & 0 & 0 & \lambda_2 \end{bmatrix} \{\epsilon - \epsilon_o\} \quad (3.20)$$

where

$$\lambda_1 = \frac{\nu}{1-\nu}\ ,\ \lambda_2 = \frac{1-2\nu}{2(1-\nu)}\ ,\ \lambda_3 = \frac{E(1-\nu)}{(1+\nu)(1-2\nu)} \quad (3.20a)$$

and $\{\epsilon_o\}$ equals residual strain vector. This equation may be written in the form

$$\{\sigma\} = [D]\{\epsilon - \epsilon_o\} \quad (3.21)$$

E. ELEMENT STIFFNESS RELATIONS

The stiffness matrix may now be assembled using the relationships given by Zienkiewicz(17) on page 16 expanded to three dimensions. The element stiffness is then

$$[K] = \int_V [B]^T [D][B] \quad dV \quad (3.22)$$

Due to the symmetry of the formulation, this volume integral may be written in terms of an area integral as follows

$$[K] = 2\pi \int_A [B]^T [D][B]\, r \; dA \tag{3.23}$$

or

$$[K] = 2\pi [C]^{-1T} \int [G]^T [D][G] r \, dA \; [C]^{-1} \tag{3.24}$$

since $[C]$ is a function of only the nodal point coordinates.

F. LOAD FORMULATION

The formulation for the load matrix contains four parts; one for each of the different ways in which loads may be applied. The four types of loading are: (1) loads due to initial strains, (2) loads due to body forces, (3) loads due to distributed surface forces, and (4) loads due to concentrated loads at the nodes. Each of these loadings are treated separately.

Nodal forces are required to balance initial strains such as may be caused by previous plastic flow or temperature changes. The formulation for these loads in two-dimensions is given by Zienkiewicz(17) on page 16 and in three-dimensions becomes

$$\{F\}_{\epsilon_o} = \int_V [B]^T [D] \{\epsilon_o\} \, dV \tag{3.25}$$

As in the case of the element stiffness matrix, this can be written in terms of area integrals and becomes

$$\{F\}_{\epsilon_o} = 2\pi \int_A [B]^T [D] \{\epsilon_o\} \, r \, dA \tag{3.26}$$

This equation can also be rewritten as was the element

stiffness matrix to remove the matrices which are not a function of the coordinates from the integral. The equation becomes

$$\{F\}_{\epsilon_o} = 2\pi[C]^{-1T} \int_A [G]^T[D]\{\epsilon_o\}\ r\ dA \qquad (3.27)$$

The initial strain matrix remains in the integral because the strain is able to take a linear form in the element when the shape function is prescribed as a full quadratic expansion. Each initial strain component is defined as being in the form

$$\epsilon_{o\ i} = a_i + b_i r + c_i z \qquad (3.28)$$

With the form of the initial strains defined, the matrices under the integral can be expanded into individual terms. The terms are evaluated using the same integrals as used for the element stiffness matrix. These are given in Appendix C.

The formulation for loads due to body forces allows for body forces due to rotation around the axis of symmetry and acceleration along the axis of symmetry. These constitute distributed loads which cause internal work. Again using the formulation of Zienkiewicz(17) on page 16 converted to three dimensions, the equation becomes

$$\{F\}_p = \int_V [N]^T\{p\}\ dV \qquad (3.29)$$

where the body load matrix $\{p\}$ defined in terms of angular acceleration ω, linear acceleration in the z-direction A_z,

and the element density ρ is

$$\{p\} = \begin{Bmatrix} \rho\omega r^2 \\ 0 \\ \rho A_z \end{Bmatrix} \tag{3.30}$$

As with the distributed load matrix, some terms may be removed from within the integral and the integration done in the form of an area integral. The equation becomes

$$\{F\}_p = 2\pi[C]^{-1T} \int_A [P]^T\{p\}\, r\, dA \tag{3.31}$$

Again the matrices under the integral are expanded and evaluated using the area integrals in Appendix C and the appropriate constants.

Distributed surface forces are allowed along any boundary of an element which is also a boundary of the structure. The three types of forces are those normal to the surface and two tangential to the surface. The directions on the tangential loads are such that one results in loads in the r and z directions and the other results in loads in the θ direction. All three loads are linearly distributed along the surface. These surface loads are expressed as

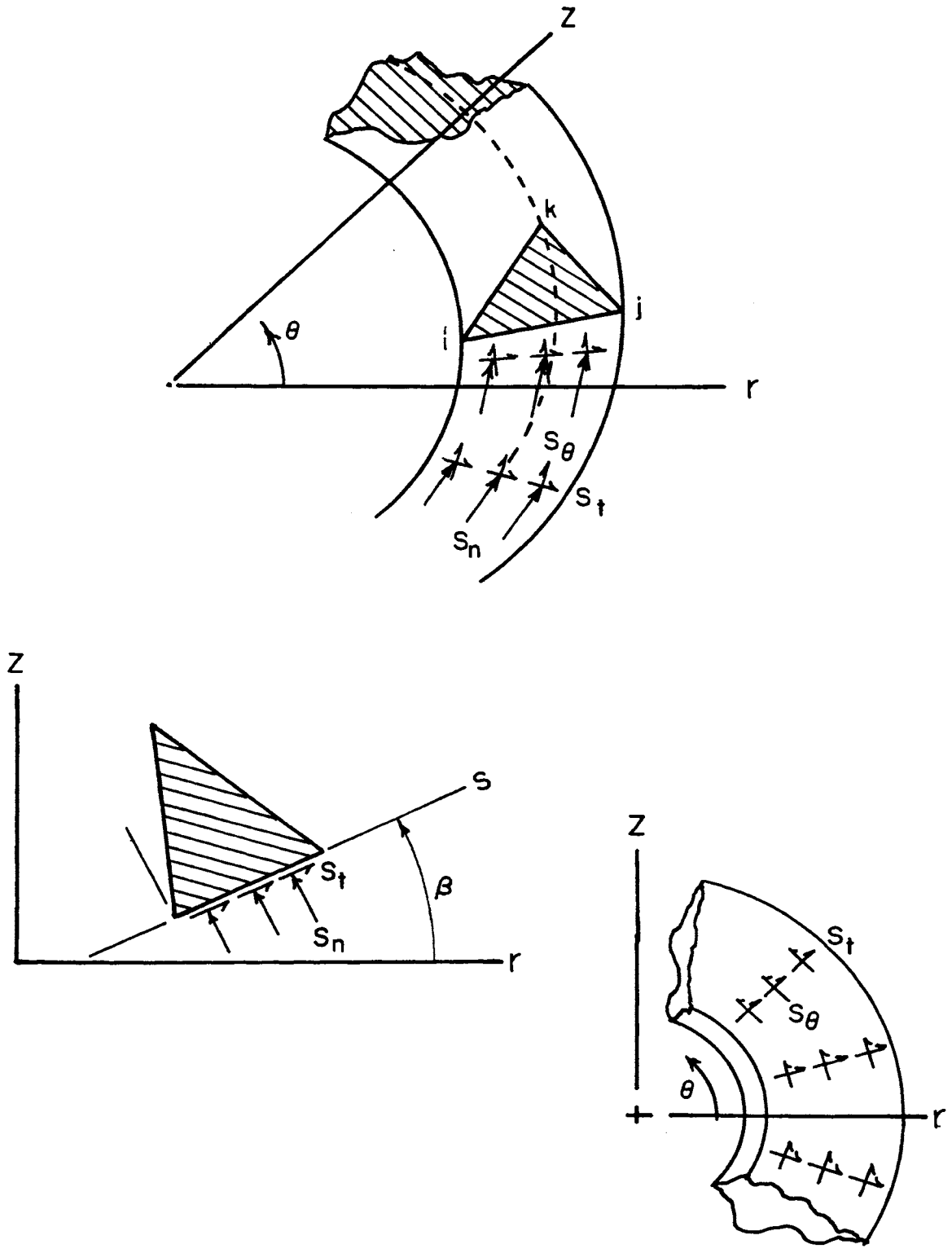

Figure 2. Typical Distributed Surface Forces on an Element Boundary

$$S_n = d_1 + d_2 s$$

$$S_\theta = d_3 + d_4 s \qquad (3.32)$$

$$S_T = d_5 + d_6 s$$

where s is the distance along the surface. Using the geometric relations shown in Figure 2, the distributed surface load matrix is

$$\{S\} = \begin{Bmatrix} -(d_1 + d_2 s)\ \sin\beta + (d_5 + d_6 s)\ \cos\beta \\ (d_3 + d_4 s) \\ (d_1 + d_2 s)\ \cos\beta + (d_5 + d_6 s)\ \sin\beta \end{Bmatrix} \qquad (3.33)$$

The load equation for these forces is the same form as the equation for body loads except that the forces are only on the surface so that integration is only along the area. The load equation due to surface loads becomes

$$\{F\}_s = \int_A [N]^T \{S\}\ dA \qquad (3.34)$$

Using the same procedures as in the case of body loads this equation becomes

$$\{F\}_s = 2\pi [C^{-1}]^T \int_S [B]^T \{S\}\ r\ ds \qquad (3.35)$$

The matrices under the integral are expanded and each term is evaluated using the integral forms given in Appendix D.

The fourth form of loads are concentrated loads at

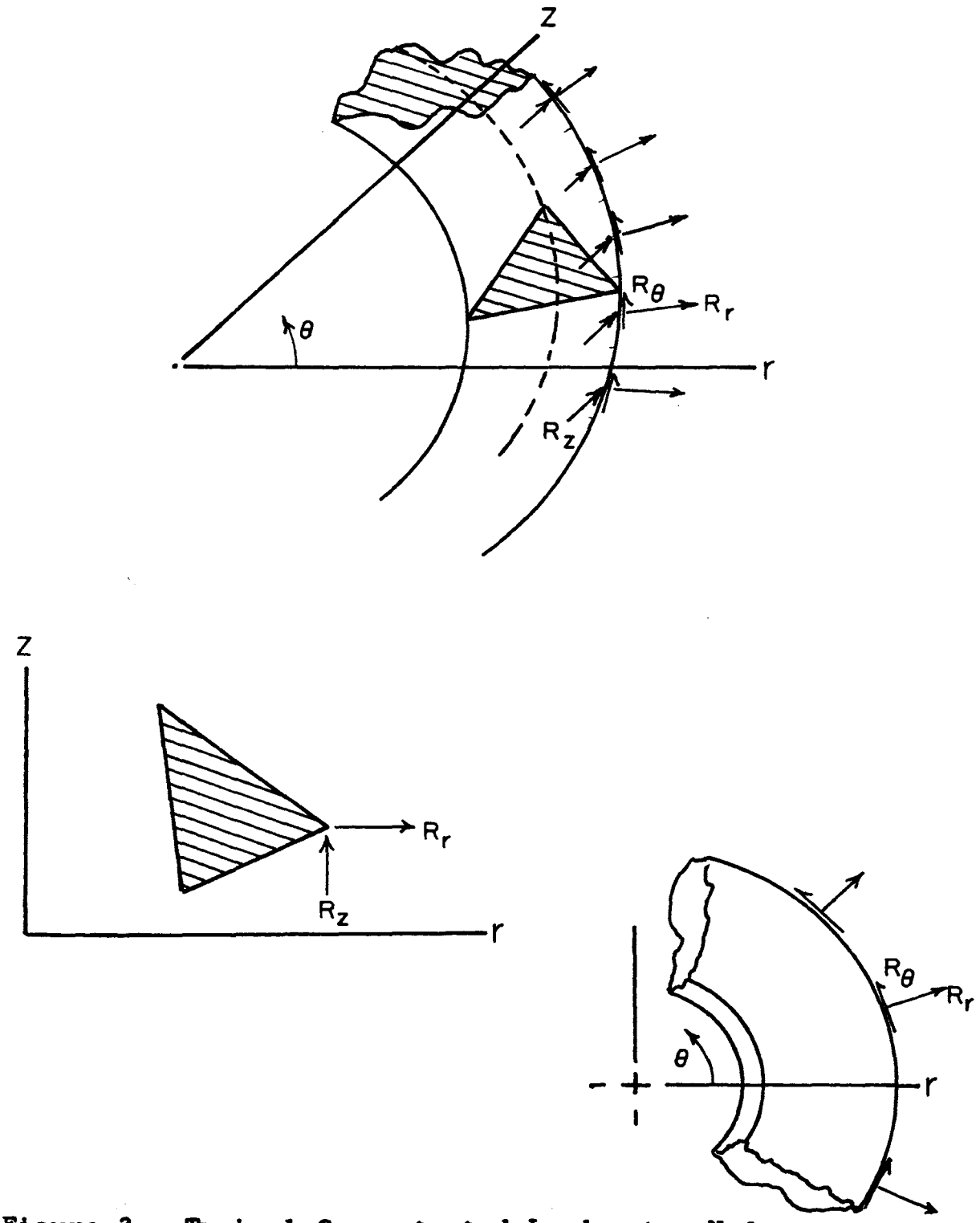

Figure 3. Typical Concentrated Loads at a Node

the nodes. The three directional concentrated loads are ring loads in the r-, θ-, and z-directions, as shown in Figure 3. These loads on the i-th node are expressed as

$$\{R_i\} = \begin{Bmatrix} R_{ri} \\ R_{\theta i} \\ R_{zi} \end{Bmatrix} \tag{3.36}$$

Since these loads are applied at each node of the element the load matrix due to concentrated loads becomes

$$\{F\}_r = \begin{Bmatrix} R_1 \\ R_2 \\ R_3 \\ \cdot \\ \cdot \\ \cdot \\ R_6 \end{Bmatrix} \tag{3.37}$$

G. MATRIX ASSEMBLY*

The assemblage of the stiffness and load matrices to form the complete nodal equilibrium equations in governed by the equation

---

*In the following sections the superscript ^{e} indicating a quantity associated with an element will again be shown.

$$[K]\{\delta\} = \{F\}_{\epsilon_o} + \{F\}_p + \{F\}_s + \{F\}_r \qquad (3.38)$$

where

$$K_{ij} = \sum K_{ij}^e$$

$$F_i = \sum F_i^e \qquad (3.38a)$$

and the i and j each indicate a degree of freedom and the summation is over all elements of the structure.

Since each node has three-directional components, therefore three degrees of freedom, three indices are associated with each node which correspond to the three equilibrium equation of the node. For a structure with 'L' nodal points, there are 3L degrees of freedom, giving the overall stiffness matrix of the structure dimensions of $[3L \times 3L]$. The indices are associated with the node in the following manner; index number (N X 3 - 2) indicates r-direction, (N X 3 - 1) indicates θ-direction, and (N X 3) indicates z-direction where 'N' is the number associated with the node.

Each element stiffness matrix $[K]^e$ has only six nodes included and must be expanded to include all the nodes of the structure before assembling the overall stiffness matrix $[K]$. This is done using the formulation of indices above and inserting zeroes for all the terms associated with nodes not on the element. In the expanded form, each element stiffness is assembled(added) into the overall stiffness matrix according to Equation (3.38a).

The load portion $\{F\}$ of the equilibrium equation requires both the addition indicated in Equation (3.38) and the assemblage over all elements of the structure. This is accomplished by summing first all of the element load matrices and then assembling the resulting matrices into an overall load matrix. The assemblage is controlled by the same index number as was used in the stiffness assemblage.

The overall nodal equilibrium equation is then expressed as

$$[K]\{\delta\} = \{Q\} \tag{3.39}$$

where

$$\{Q\} = \{F\}_{\epsilon_o} + \{F\}_p + \{F\}_s + \{F\}_r \tag{3.39a}$$

This expression is the system of equations which describes the nodal displacements. It is noted that a constant value of 2π appears in all the evaluations of these matrices, except $\{F\}_r$ which is due to concentrated loads. Therefore all the terms in Equation (3.38) are divided by 2π to simplify the calculations.

When assembling the overall stiffness, two modifications were made in order to conserve fast access computer storage. The first modification utilizes the symmetry of the elastic stiffness matrix. Only the upper half triangular portion of the stiffness matrix must be stored.

The second modification bands the stiffness matrix by restricting the maximum difference of the nodal numbering system within an element. This bandedness is possible because the equation index is associated with the node number. All elements of the stiffness matrix outside the band are zero and therefore need not be stored. The non-zero elements of the stiffness matrix are then stored such that the diagonal elements form the first column of the matrix storage form. The bandedness then permits the exclusion from storage, of all the elements outside the prescribed band width. An element of the stiffness matrix was stored using the transformation

$$k_{ij} = k_{mn} \tag{3.40}$$

where

$$\begin{aligned} m &= i \\ n &= j - i + 1 \end{aligned} \tag{3.40a}$$

and where i and j are indices of the stiffness matrix, and m and n are indices of the stored form.

H. MODIFICATIONS DUE TO BOUNDARY CONDITIONS

Certain modifications to the overall stiffness matrix and overall load matrix are necessary due to the boundary conditions imposed on the structure. There are two types of conditions which must be met.

The first condition is that displacements in the

angular and radial directions must be zero along the axis of symmetry. The angular requirement is imposed to eliminate a displacement around the axis at a zero valued radius. The radial requirement is necessary to ensure continuity at the axis.

The second condition is that a displacement may be specified for any node or any node direction. This displacement must be specified in the input information defining the structure. There must be some combination of nodal displacements specified to prevent rigid body motion of the structure.

The method of imposing both of these conditions on the overall stiffness and load matrix is the same so only one procedure is outlined. The known displacement is inserted into the overall stiffness in such a manner that the energy conditions of the overall system of equations is retained and that the equation containing the known nodal displacement will yield the prescribed value when the system of equations is solved. The modification is done in two parts. The first part is to modify the equation for the node imposing the prescribed displacement. The energy due to the displacement of the node is subtracted from the load element of the equation. This is evaluated by multiplying the known nodal displacement by the element of the nodal stiffness equation which indicates the load at the node due to a displacement of this node. Then this same element is set equal to one

and all other elements of that nodal stiffness equation are set to zero, as they cannot influence its displacement. The second part of the modification is to adjust the load element of all of the other nodal displacement equations to reflect the known displacement. This is accomplished by subtracting from the load element of each of the nodal displacement equations, the value of the known displacement multiplied by the element of the nodal stiffness equation which indicates the load on the affected nodal equation due to the known node displacement. Then this stiffness element is set to zero since its effect was transferred to the load portion of the equation.

I. EQUILIBRIUM EQUATION SOLUTION

The nodal displacement equilibrium equation given as equation (3.38) contains a symmetrical positive-definite stiffness matrix and two column matrices and is

$$[K]\{\delta\}=\{Q\} \tag{3.41}$$

The technique applied to solve for the displacement matrix is the "Cholesky Method" as given by Fox(22). This method was used on the modified matrix forms which are described in the section Matrix Assembly.

A short review of the "Cholesky Method" is described in terms of the particular equations to be solved. The stiffness matrix $[K]$ is reduced such that

$$[K] = [L]^T[L] \tag{3.42}$$

where $[L]$ is non-zero only in the upper half triangular matrix. From this, the elements of the reduced matrix $[L]$ are defined in general indices i and j as

$$\begin{aligned} l_{ii} &= \left(k_{ii} - \sum_{r=1}^{i-1} l_{ri}^2 \right)^{1/2} \\ l_{ij} &= \frac{1}{l_{ii}} \left(k_{ij} - \sum_{r=1}^{i-1} l_{ri}\, l_{rj} \right) \end{aligned} \tag{3.43}$$

Only the upper half triangle of $[K]$ is stored. Also, only the upper half triangle of $[L]$ is non-zero and must be retained. Therefore, $[L]$ is shifted in the same manner as $[K]$, as was outlined in Matrix Assembly, and is given as

$$l_{ij} = l_{mn} \tag{3.44}$$

where the stored indices m and n are

$$\begin{aligned} m &= i \\ n &= j - i + 1 \end{aligned} \tag{3.45}$$

With this shift, the elements of $[L]$ are defined by

$$l_{m1} = \left(k_{m1} - \sum_{r=1}^{m-1} l_{r,\, m-r+1}^2 \right)^{1/2}$$

$$l_{mn} = \frac{1}{l_{m1}} \left(k_{mn} - \sum_{r=1}^{m-1} l_{r,\, m-r+1} \; l_{r,\, m+n-r} \right) \tag{3.46}$$

An element of the stiffness matrix $[K]$ is not required for calculation except when evaluating the reduced stiffness matrix $[L]$. Therefore, this storage area is released at the completion of the procedure.

The next step in the solution is the forward substitution for the stiffness matrix $[K]$ defined in Equation (3.42) into the equilibrium equation given in Equation (3.41). The result is

$$[L]^T[L]\{\delta\} = \{Q\} \tag{3.47}$$

Then letting a new substitution load matrix $\{Y\}$ be defined as

$$\{Y\} = [L]\{\delta\} \tag{3.48}$$

the equilibrium equation becomes

$$[L]^T\{Y\} = \{Q\} \tag{3.49}$$

From the equilibrium equation the elements of the substitution load matrix $\{Y\}$ are defined in general indices as

$$y_i = \frac{1}{l_{ii}} \left(q_i - \sum_{r=1}^{i-1} l_{ri} \; y_r \right) \tag{3.50}$$

This equation is converted to the storage indices defined in Equation (3.45) and becomes

$$y_m = \frac{1}{l_{m1}} \left(q_m - \sum_{r=1}^{m-1} l_{r,\, m-r+1} \; y_r \right) \tag{3.51}$$

An element of the load matrix $\{Q\}$ is required for calculation only when an element of the substitution matrix $\{Y\}$ of the same row is evaluated. Therefore, the storage is released for use by the element of the substitution matrix $\{Y\}$.

The last step of the solution is the back substitution procedure. Equation (3.48), which defines the substitution matrix $\{Y\}$ is solved for the displacement matrix $\{\delta\}$ whose elements in general indices become

$$\delta_i = \frac{1}{l_{ii}} \left(y_i - \sum_{r=i+1}^{s} l_{ir} \, \delta_r \right) \tag{3.52}$$

where s is the total number of equations. This equation is also converted to storage indices by Equation (3.45) and becomes

$$\delta_m = \frac{1}{l_{m1}} \left(y_m - \sum_{r=m+1}^{s} l_{m,\, r-m+1} \; \delta_m \right) \tag{3.53}$$

From the equation it is seen that an element of the substitution matrix $\{Y\}$ is required for calculation only for the element of the displacement matrix $\{\delta\}$ of the same row, so the storage location is released for use by the displacement matrix $\{\delta\}$ element.

In order to conserve fast access or core computer storage space, the equilibrium equations were not solved by operating on the equation with all elements in core storage. Instead, the overall stiffness matrix $[K]$ was broken up into submatrices to form a column matrix at the time of assembly. These submatrices were stored in magnetic disk storage. All submatrices were generated before the solution procedure began.

The procedure of solution was to move the first submatrix into core storage, and perform the manipulations indicated in the reduction procedure. These were carried out only for the elements of the submatrices. Then, the forward substitution procedure was done for the same submatrix. The reduced form of the stiffness was then placed into disk storage. The elements of the reduced stiffness were also retained in core for use in the next step. The next stiffness submatrix was loaded into the core area formerly occupied by the first stiffness submatrix and the reduction and forward substitution repeated for this submatrix. The reduced elements were placed into locations occupied by the reduced elements of the previous step.

This was acceptable, due to the order in which the elements of the previous reduction were required for evaluation of the new reduced elements. This process proceded from one submatrix to the next until the whole system of equations had been reduced and the forward substitution completed.

The back substitution process was started in the last submatrix on the last equation. The procedure was performed on subsequent equations thru to the first equation of the submatrix. Then the next submatrix was returned from disk storage, and the procedure progressed in the same manner. This process was repeated until all equations had been back substituted. The solution for the displacements was then complete.

J. THE PROGRAM

The computer program for the axisymmetric three dimensional solid was written to solve a general structural problem of this form. This requires that the program have the capability to solve complex problems without requiring an unreasonable amount of fast access computer storage. Another requirement is that the solution does not require an excessive amount of computer time. The program was written so that the fast access storage requirement can be fairly easily changed to fit the computer system available without requiring a limitation on the size of the problem capability. This is done by using

some form of bulk storage, preferably disk storage. The program has not been optimized in many respects, but many aspects of the program are written to conserve computer time. The program was executed on the University of Missouri - Rolla computer system, which is an IBM 360, Model 50, with IBM Model 2314 Disk Storage. The program does not require the total storage capability of this system, but does require 252 K core storage and one disk drive unit.

The program was written in "FORTRAN" Language(23) and is in two job steps in order to make a maximum use of the available core storage. The first step is the generation of the displacement equilibrium equations from the input data. The input data required is an abbreviated form of the information describing the structure under investigation. The remainder is generated by the program on the basis of the input information. From this data the equilibrium equations are generated. The equations and all the structure description information are then placed in disk storage. The second step retrieves the stored information and performs the process of solution. The displacement solutions are then used to evaluate their associated strains and stresses. The form of output of the desired information is controlled by the second step. The program outline is given in Figures 4 thru 8.

K. COMPUTATION EFFORT

The total solution time depends, of course, on the number of elements employed in the descretization of the structure and, even more significantly, on the number of nodal points. The number of nodal points determines the total number of equations contained in the equilibrium equation system. Typical computational times for the various structures studied, which does not include the time required for the compilation of the "FORTRAN" language, are given below.

NUMBER of NODES	NUMBER of ELEMENTS	COMPUTATION TIME (minutes)	AVERAGE TIME PER NODE (minutes)
227	96	6.27	0.0276
249	102	7.53	0.0302
305	128	10.52	0.0345

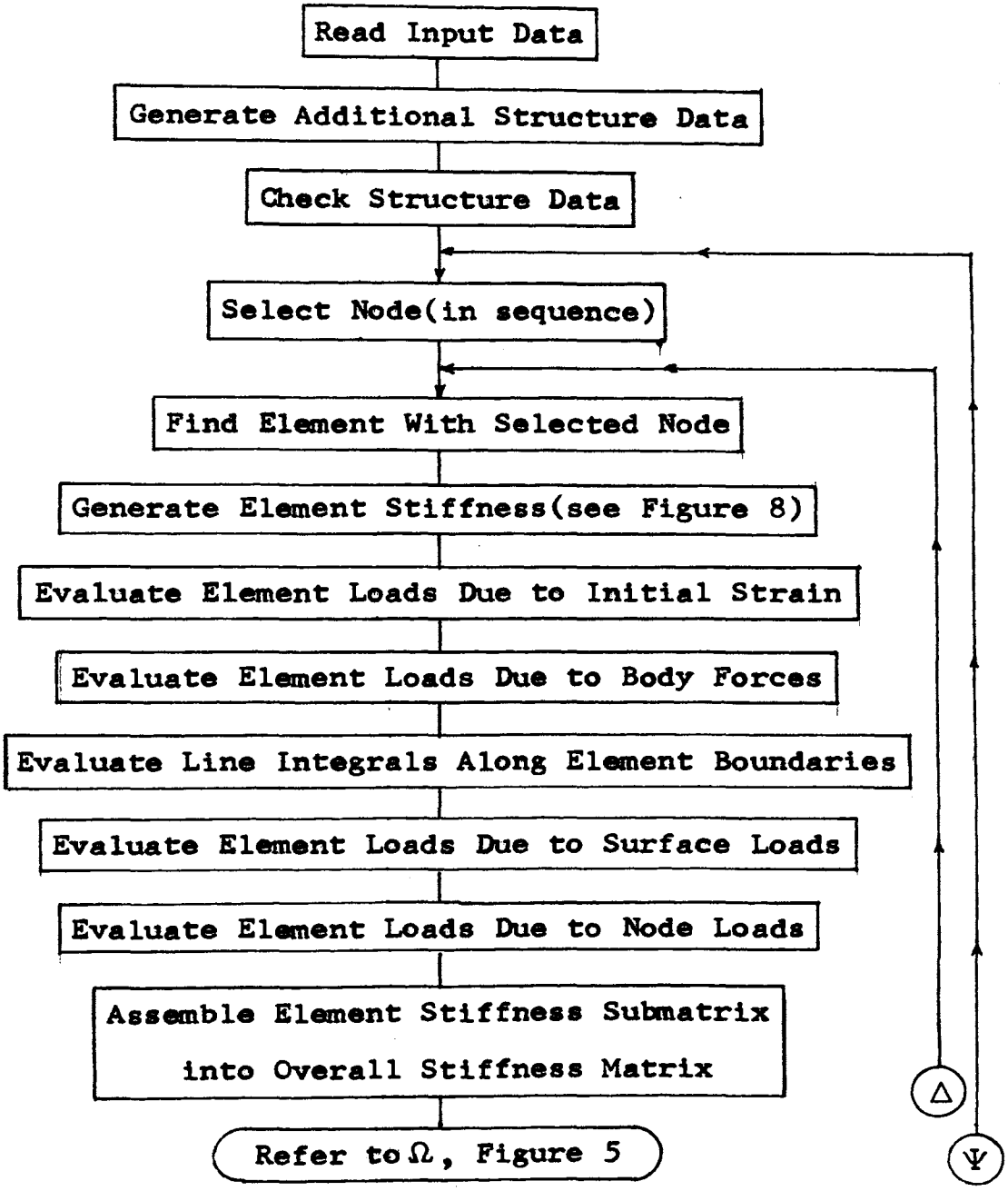

Figure 4. Program Outline for the Axisymmetric Finite Element Method -- Step One

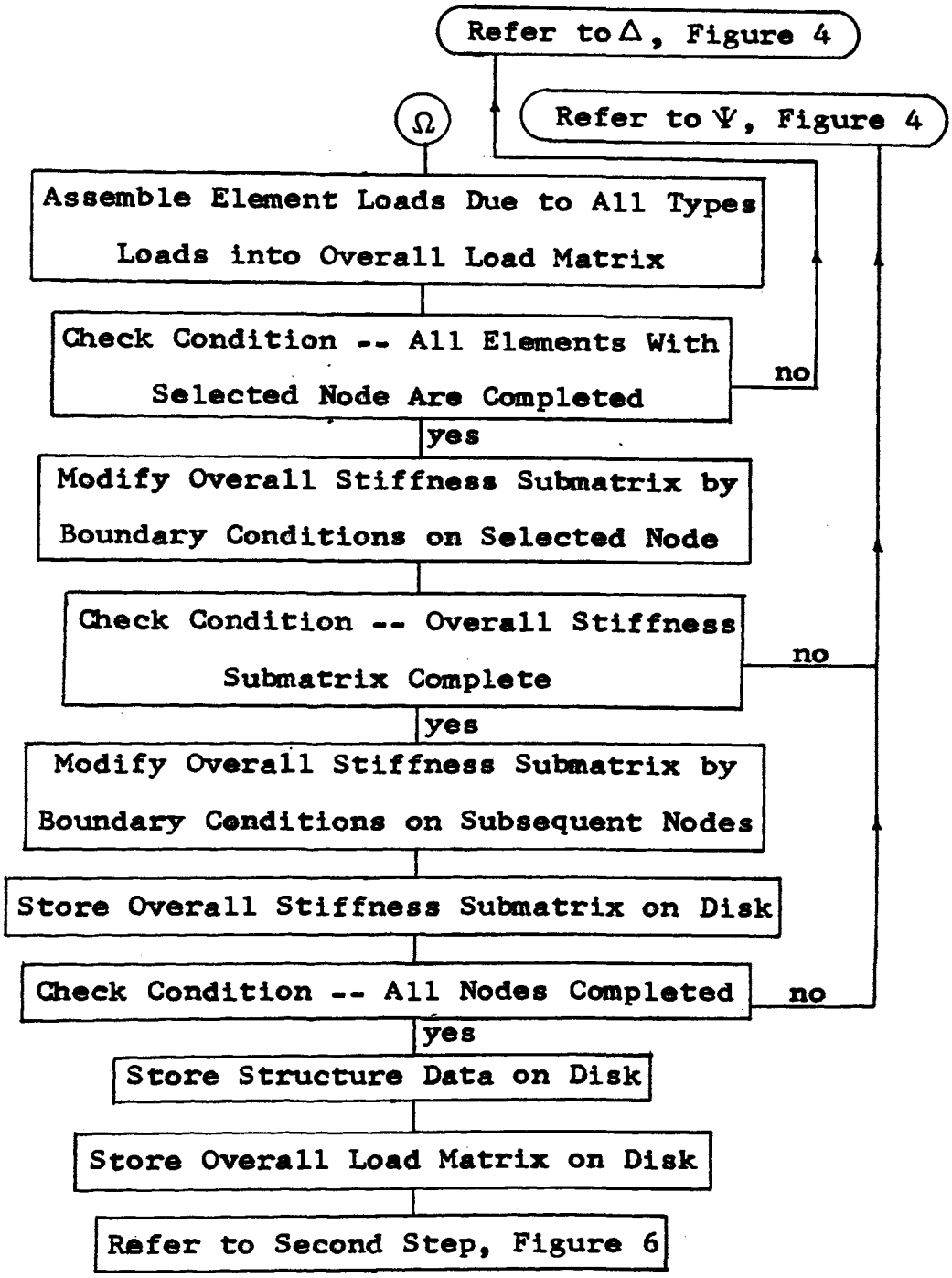

Figure 5. A Continuation of the Program for the Axi-Symmetric Finite Element Method -- Step One

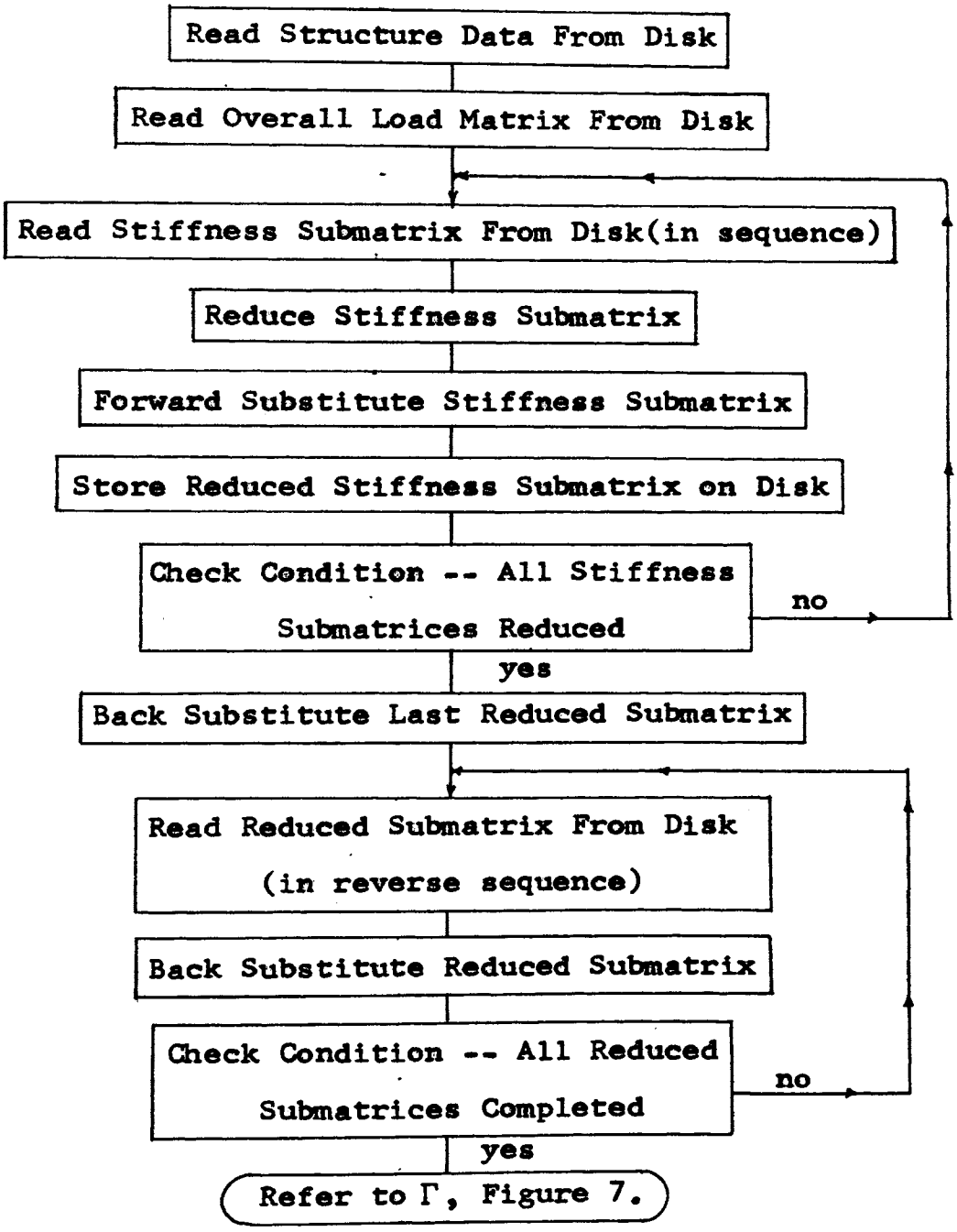

Figure 6. Program Outline For the Axisymmetric Finite Element Method -- Step Two

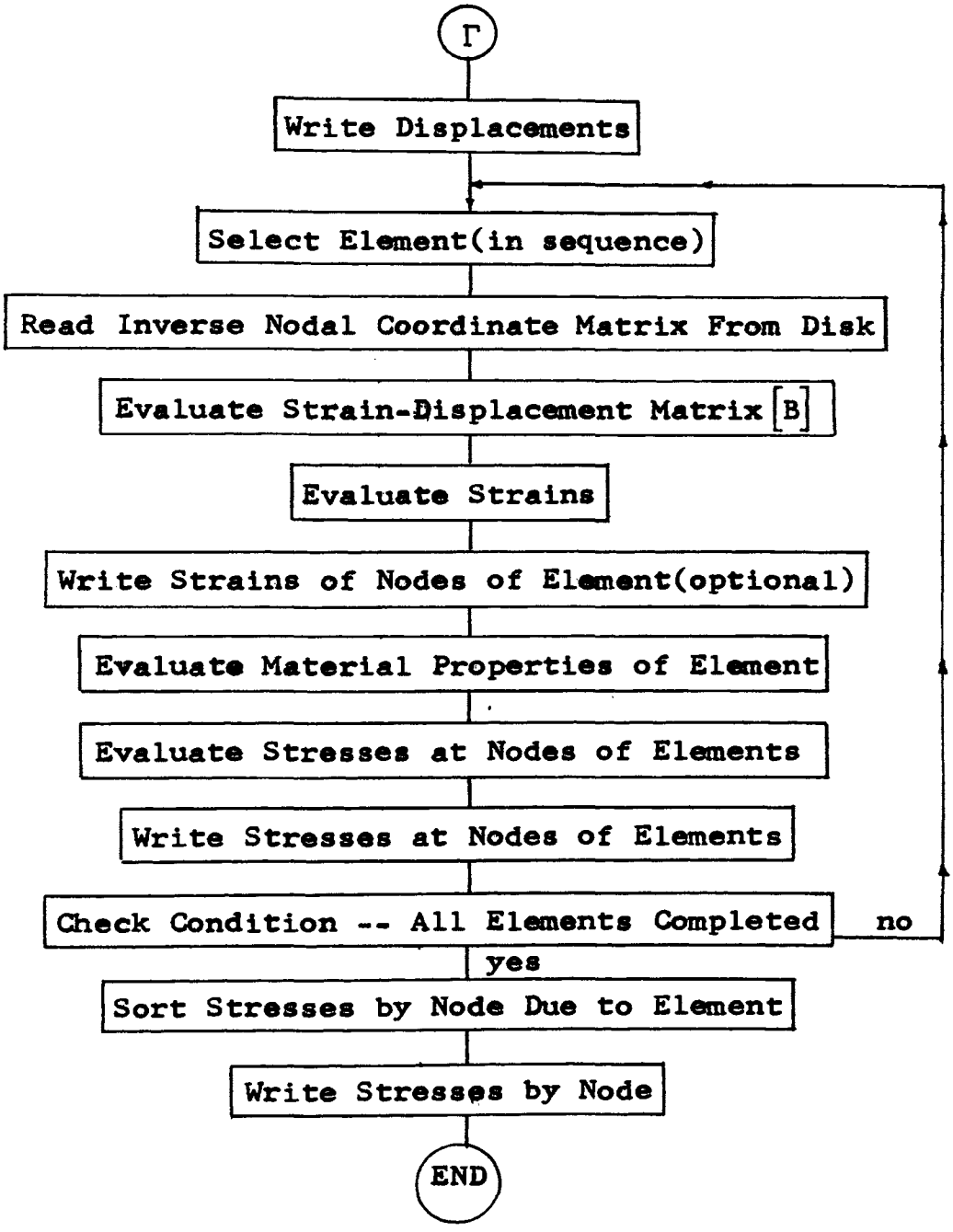

Figure 7. A Continuation of Program Outline For the Axisymmetric Finite Element Method -- Step Two

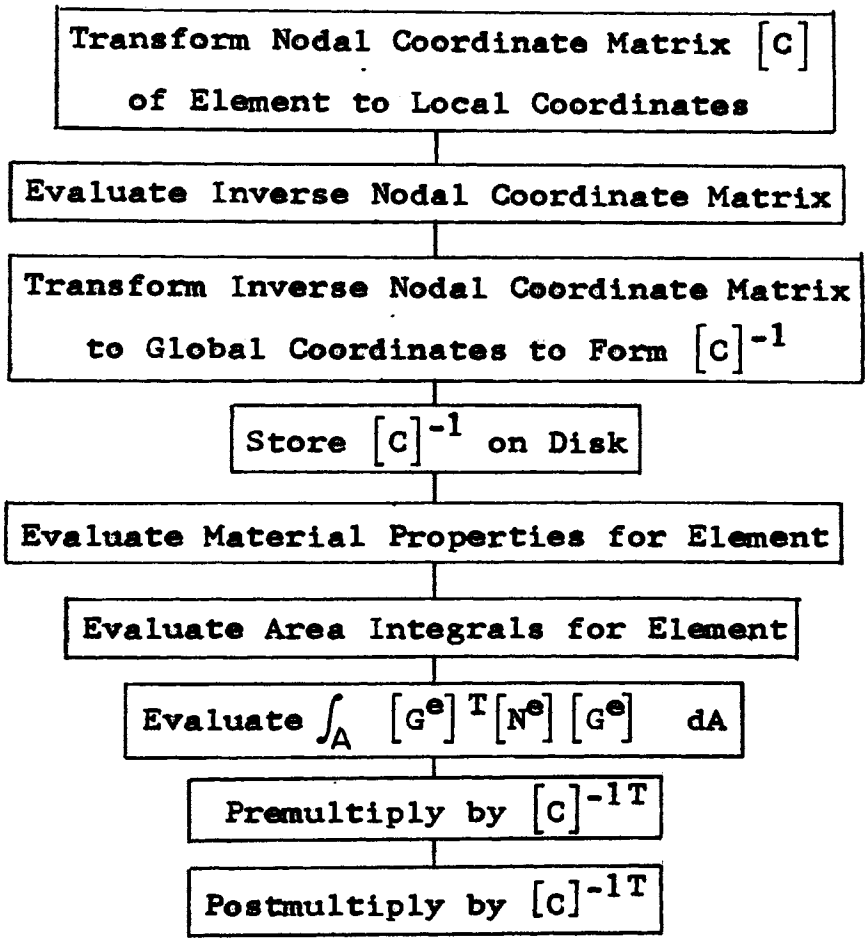

Figure 8. Outline of Element Stiffness Generation

L. STRUCTURES INVESTIGATED AND RESULTS

Three structural geometries were studied by the finite element method. Two structural geometries corresponded to extremes of the experimental specimen geometries tested. A third specimen geometry was in the middle of the test specimen group.

The geometry used for the finite element analysis was not the complete geometry of the experimental test section, but a geometry which can be translated to a form suitable for comparison. The first geometry was simply a stepped shaft section in which the shaft was extended far enough away from the step portion so that its stresses and displacements were that of a simple shaft. The second and third geometries used were samples of the shaft across the disc section. Again they were extended to the point of a simple shaft.

The discretized structures and the flexibility of each are given in Figures 9, 10, and 11.

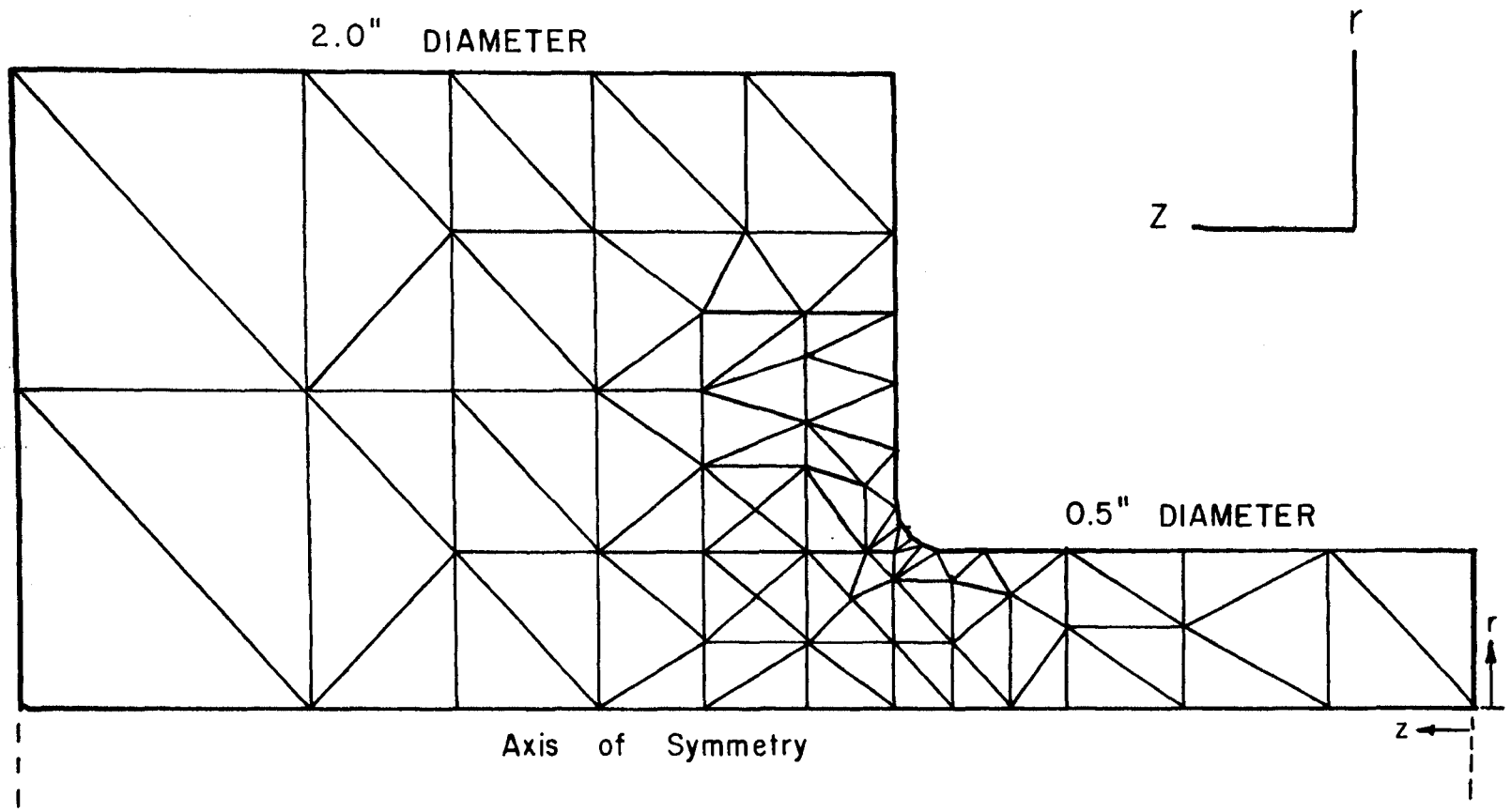

FLEXIBILITY —— 0.42953 x 10^{-4} radians / inch - pound

Figure 9. Discretized Step Shaft, 0.5 to 2.00 Inch Diameter

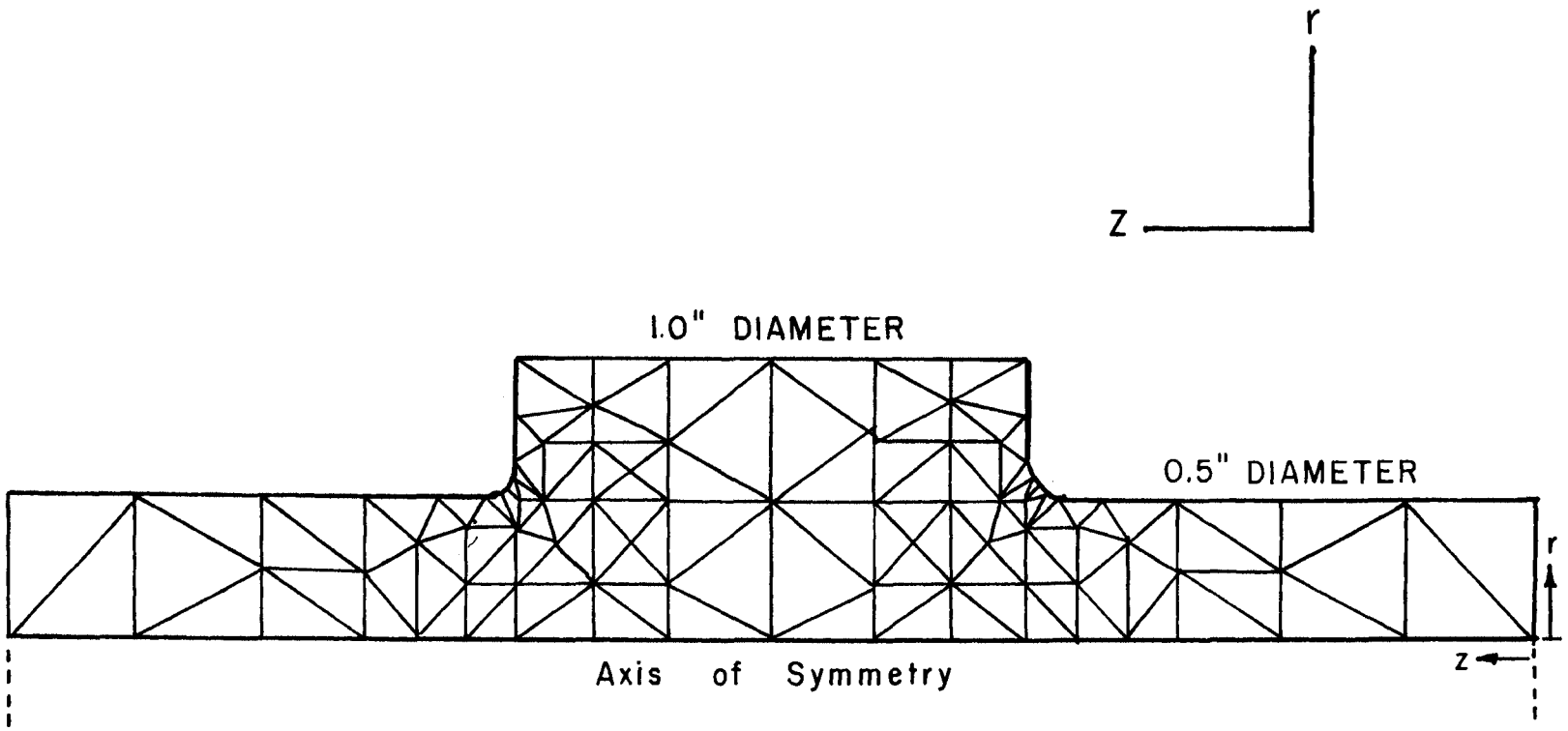

FLEXIBILITY —— 0.88978×10^{-4} radians / inch - pound

Figure 10. Discretized Disked Shaft, 0.5 to 1.00 Inch Diameter, 1.0 Inch Width

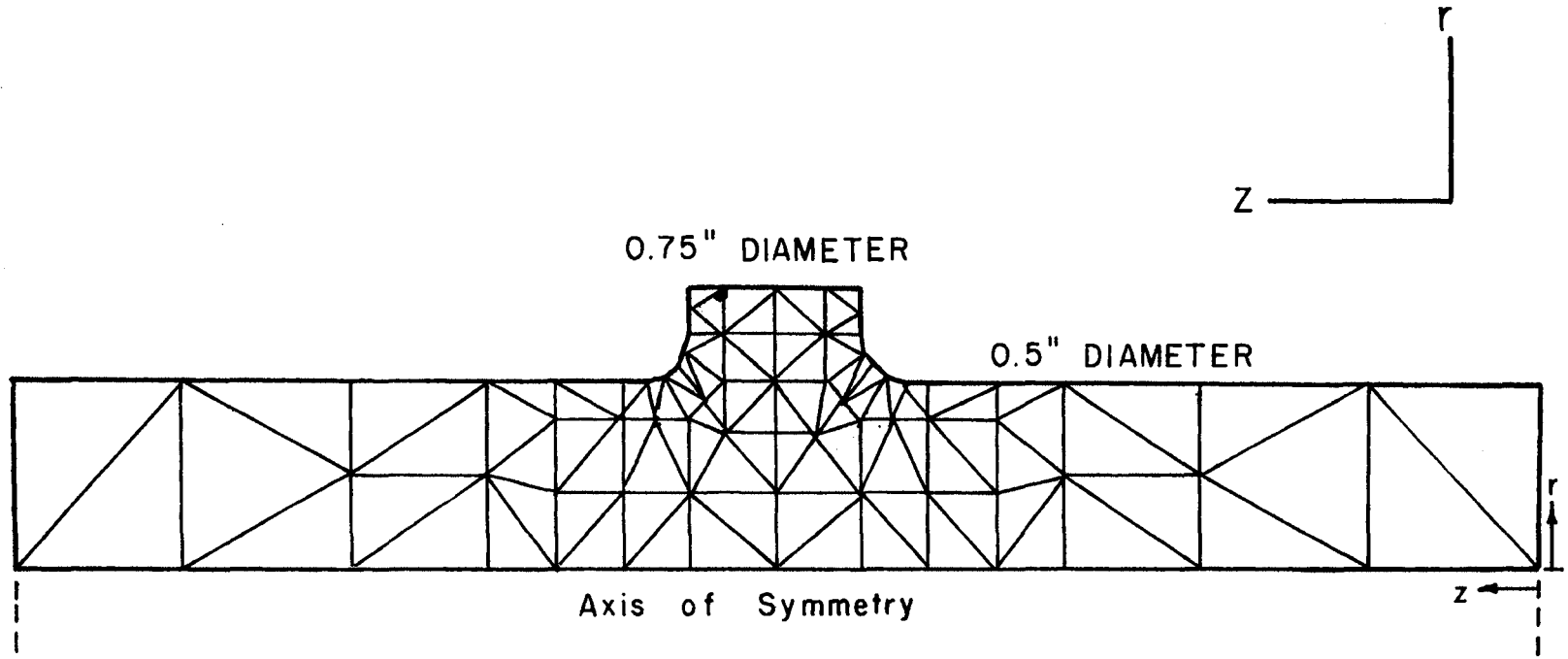

FLEXIBILITY —— 0.84589 x 10^{-4} radians / inch - pound

Figure 11. Discretized Disked Shaft, 0.5 to 0.75 Inch Diameter, 0.125 Inch Disk Width

CHAPTER IV

EXPERIMENT

A. TORSION TEST MACHINE

The precision torsion test machine was designed and built as part of this research for the University of Missouri - Rolla. The machine is designed for the testing of relatively small specimens(two feet long) and is capable of applied torques up to 600 inch-pounds.

1. TEST FRAME

The frame is designed to hold the test specimen axis in the vertical position, to facilitate the angular measurements and to provide the rigidity needed to apply the loads. Since the specimen holders isolate the specimen from flexure of the frame, an extremely rigid frame is not required.

The entire frame stands on a three point contact with the floor, allowing vertical alignment of the frame. This alignment is used in conjuction with the angular measurement.

2. SPECIMEN HOLDERS

In designing the specimen holders, it was necessary to consider an attachment method which allowed transmission of the applied torque while minimizing any transmitted bending or axial load. This is accomplished with flexible Hooke Joints and a longitudinal slip joint between the frame and the specimen.

The upper frame unit is rotationally and axially fixed, with a flexible joint between the upper frame and the specimen. A one inch hexagonal socket on the flexible joint is used to clamp the specimen. The lower frame unit is both a specimen holder and the support for applying the torque. The loading shaft through the lower unit is supported by two ball bearings and has a flexible joint with a hexagonal socket at the upper end. The hexagonal socket engages the specimen and slippage is allowed in the axial direction. The lower end of the loading shaft is attached to the moment arm.

3. TORQUE LOADING

The torque is applied through a moment arm attached to the loading shaft of the lower frame unit. The force is applied to the moment arm through a hardened ball nose pin in the arm. This arrangement has a measurable and unvarying moment arm length. The pin rests against a hardened plate on the force transducer. Both the transducer and the plate are rotatable around the axis of the loading shaft, so that the plate remains perpendicular to the pin. Thus, the load applied to the pin is perpendicular to the moment arm and the forces sensed by the transducer are all torque producing. The forces are applied through rotation of the transducer assembly around the axis of the loading shaft by advancing a swivelling lead screw between the transducer assembly and the frame.

B. LOAD INSTRUMENTATION

The loading torque is achieved by applying a force on a fixed length moment arm. The force is measured by a linear variable differential transformer load cell,* with a capacity from zero to one hundred pounds. The transducer-amplifier system* for the load cell is coupled to a digital null voltmeter* through a secondary amplifier. The original load sensing system has an accuracy of plus or minus one pound. Using the digital readout arrangement instead of the meter readout of the transducer-amplifier unit, the accuracy is extended to plus or minus one-tenth pound.

A calibration fixture was built in order to establish the workable limits of the load measurement system and to check and establish the calibration for each run. Re-calibration is necessary because the measurement system's temperature sensitivity becomes influential when the limits of accuracy are extended.

C. ANGULAR DISPLACEMENT MEASUREMENT

The angular displacement of the specimen is determined by measuring the linear displacement of a moment arm. The optical system used is similar to that used on sensitive galvanometers with a gas laser produced light beam.

---

*Commercial equipment is listed in the Equipment List on page 112

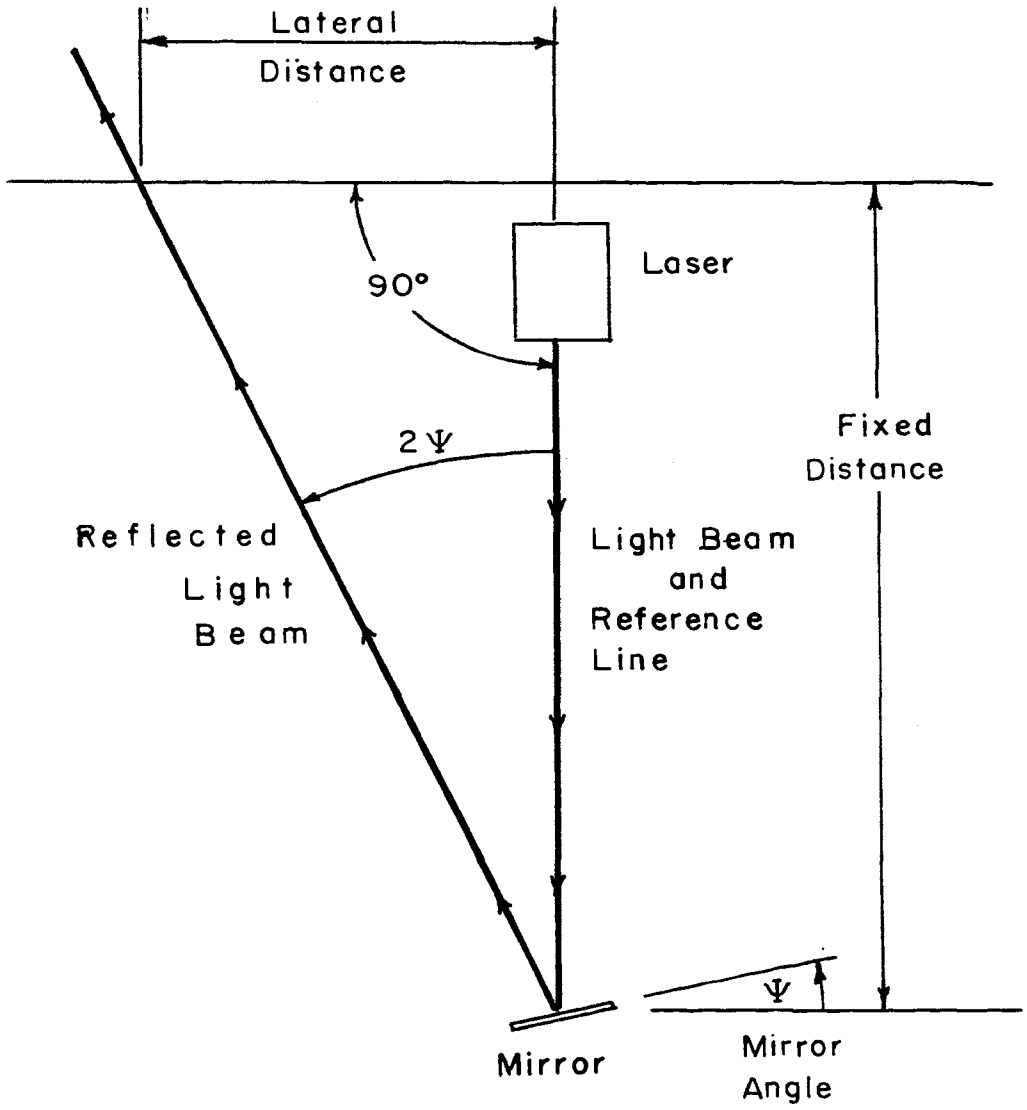

Figure 12. Diagram of the Angular Measurement System

The measurement system consists of a specimen gage with attached mirrors, a laser light source, a light beam scanner, and a calibrated displacement gage.

1. THEORY OF OPERATION

The angle between two lines in a plane may be found by the measurement of the two sides forming the tangent of the angle and taking the inverse of this tangent to find the angle. The lines, in this case, are the beam of light from the laser projected onto a first surface mirror and the beam reflected from this mirror. The angle formed between these beams is twice the value of the angle between the projected light and a line normal to the surface of the mirror. A double angle is obtained because the angle of incidence equals the angle of reflection on a plane mirror.

The line of the projected beam establishes the reference from which all angles are taken. A line set at right angles to this reference line establishes the third side of the right triangle. The distance measurements are taken along these two lines. The length along the projected beam remains constant and the length along the third varies with the angle. This length is denoted as the lateral distance.

The desired measurement is the angle of twist of the specimen under various applied loads. In order to eliminate

the effect of the specimen holders, the angle of twist is measured between two points on the specimen. This requires two angular measurements for each load. Each measurement is taken with respect to the reference line.

To obtain the two angles, two mirrors are attached to the specimen at appropriate locations. Each mirror requires a measurement system. To eliminate the need for two independant and separate systems, the system is arranged so that most of the components of the measurement system are common to both. This is accomplished by moving the projected beam from one mirror to the other as the angle of each is required. To minimize the amount of adjustment of the light source necessary to accomplish the switching, and to have the reflected beam in each case at about the same height, the mirrors are held in an immediately adjacent position by the specimen gage.

The distance along the reference line is fixed and is measured from the center of the displacement gage at its axis to the center of the specimen. The axis of the displacement gage forms the line along which the lateral distance is measured, and the distance between the reference line and the reflected beam crossings of this axis is the lateral distance. The crossing point is detected by the light beam scanner which is mounted on the traveling table of the displacement gage.

2. SPECIMEN GAGE

The specimen gage performs several functions: (1) provides a means of securing the gage to the test specimen, (2) provides support for the mirrors such that they are adjacent, and each rotatable with its attachment points on the specimen, (3) provides a means of controlling the distance between attachment points, giving a constant gage length.

The gage is made in two sections, one for each of the two measurement systems. Each section is in two parts to form a split case, so that the gage can be attached to the specimen and surround it. Each of the sections has a set of attachment points and a mirror.

The attachment points are at the upper end of the larger or upper section and behind the mirror in the smaller or lower section. Each attachment to the specimen is accomplished with three pins spaced around the specimen at 120 degrees. Two of the pins have a flat face on the end which rests against the specimen. The third pin is ground to a sharp point and is forced into the surface of the specimen to provide solid attachment at a concentrated point.

The mirrors are attached to one part of the split case of each section. Each mirror has a 25 by 35 millimeter area with an aluminized front surface and is 6 millimeters thick. The mirrors rest against a foam

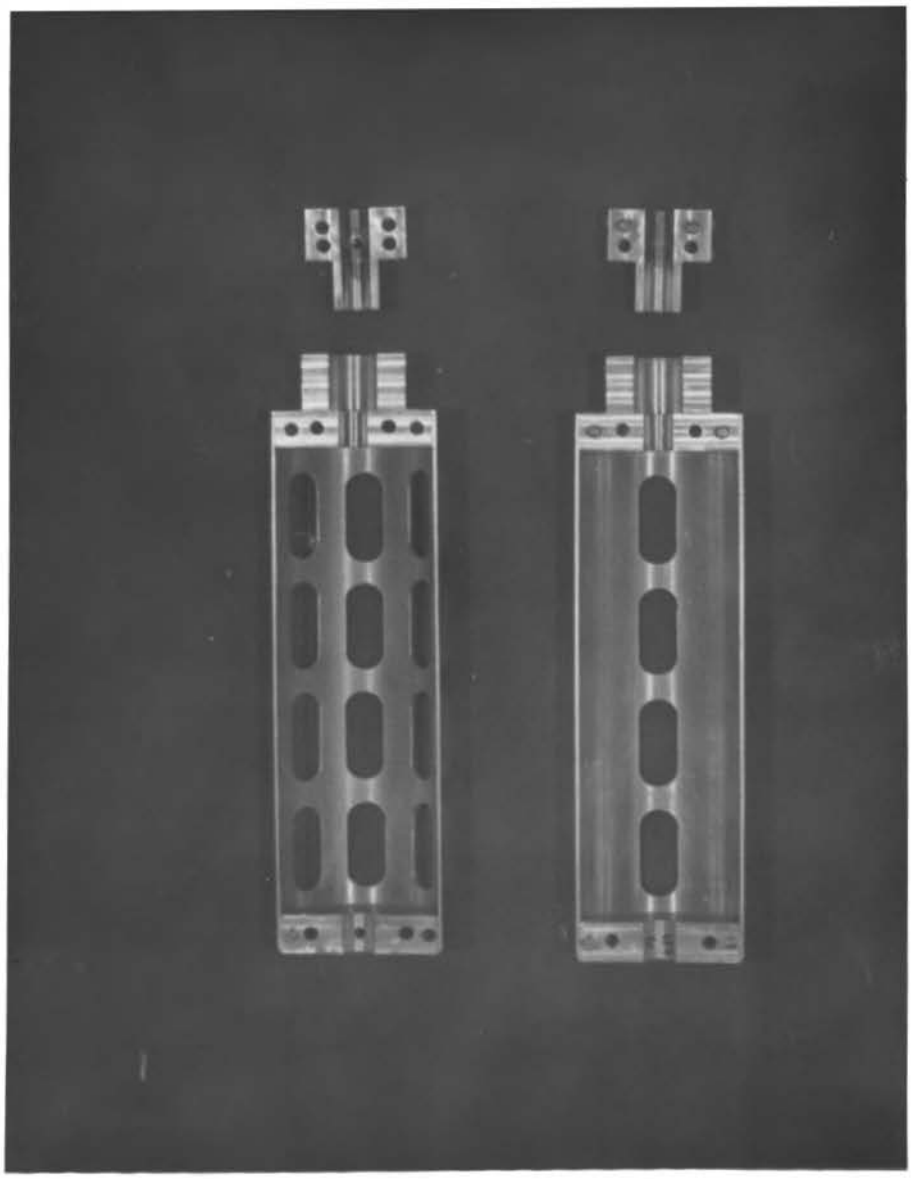

Figure 13. A Photograph of the Specimen Gage

material in the back of the holders and are held in their respective pockets in the case by four washers positioned at the mirror corners. This arrangement provides secure holding and at the same time introduces no force which can distort the mirror.

The reflecting surface of the mirror is not in line with the axis of rotation of the specimen but set away from the axis 0.500 inches. This causes the mirror to translate as well as rotate with the rotation of the specimen. The translation causes a slight foreshortening of the fixed distance along the projected beam as the specimen is rotated from a central position. The foreshortening is very small compared to the original fixed length of 140 inches, therefore, this small error is neglected.

The upper section is constructed so that it extends down to the area of the lower section and provides the support for the mirror in a location immediately above that of the lower mirror. This extension is the large tubular part of the upper section.

Since the gage is constructed with the two sections adjacent in the area of the mirrors, by controlling the amount of separation between the sections at this point, the gage length or distance between the attachment points can be controlled. This space is held constant by using a spacer between the two sections during the mounting of the specimen. This prevents the two gage sections from

actually touching. The gage length is ten inches.

3. LIGHT SOURCE

The light source is a continuous wave gas laser* which is mounted so that the beam can be easily aimed.

The laser output is 6328 angstroms, red light, continuous wave with one milliwatt power. With the optics used, the beam has a divergence of 0.7 milliradians which gives only a slight increase in the diameter of the beam over the distances used.

The laser is mounted on a frame which is rotatable in both the horizontal and vertical plane. These adjustments are used to align the beam with the reference line to accomplish the switching of the beam between the two mirrors.

4. DISPLACEMENT GAGE

A displacement gage is used to measure the lateral distance from the reference beam to the reflected beam. The gage consists of a traveling platform and the rail upon which the platform moves. The movement of the platform on the rail is measurable along the axis of the rail.

The platform of the gage is attached on the rail by four ball bearings contained in grooves in the rail sides.

---

*Commercial equipment is listed in the Equipment List on page 112

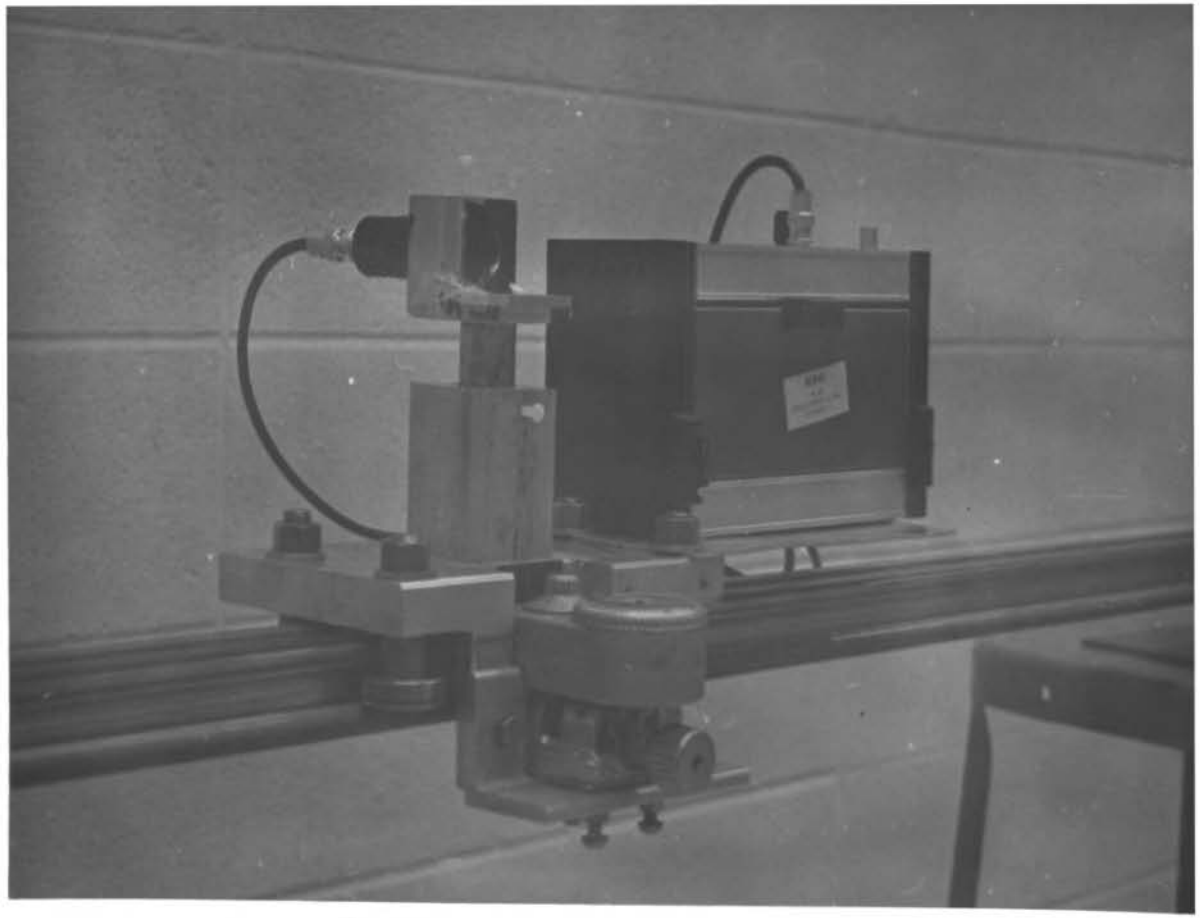

Figure 14. A Photograph of the Displacement Gage

The relative distance of platform travel is measured with a gage* engaging the rail with a smooth wheel pressed against the rail. The rail is aligned at right angles to the reference line and the travel of the platform is measured from a reference point at one end of the rail.

The traveling platform holds the light beam scanner, which provides a means of locating the reflected beam. The transducer of the scanner is in a holder on the platform. The holder allows the scanner to be raised, lowered, and rotated without affecting its position laterally, thus allowing the scanner to be aimed at the light beam.

5. LIGHT BEAM SCANNER

The light beam scanner is used to find the point at which the reflected beam crosses the axis of the displacement gage. The unit is a modified optical power meter.*

In operation, the power meter is used to detect the level of light input of the reflected beam. The level of input is used to detect the amount of offset between the center of the light beam and the center of the scanner transducer. By returning to the same power level, the offset is held constant and the lateral distance is varied only by movement of the traveling platform of the displacement gage.

---

*Commercial equipment is listed in the Equipment List on page 112

It was found that the laser light beam power has an approximate normal statistical distribution with the offset distance, when cut off by a vertical knife edge centered on the transducer. By selecting a reference power level in the region of maximum slope of the power distribution curve, a maximum sensitivity to the offset is obtained.

The power level curve is affected by the angular alignment of the transducer with the beam. To align the transducer for best light signal reception, an alignment gage is substituted for the transducer in the transducer holder. The alignment gage is a tube with a translucent window in the end. The holder is maneuvered until the beam is aligned between the knife edge and a point on the window. After alignment of the holder, the transducer is replaced in the holder, and the power level is set to the reference point by adjustment of the displacement gage.

D. TEST SPECIMENS

The test specimen material was chosen for consistent properties, high strength, and low modulus of rigidity, so that a maximum deflection could be obtained. The material selected was a high strength aluminum.

The specimens were made so that each configuration of disks could be used for several different tests. The diameter of each disk was machined smaller after each

test was completed, to give a new configuration for another test. After the complete series of tests, the disks were entirely removed. This plain rod was used to experimentally determine the Modulas of Rigidity of the specimen.

Multiple disks were used to give a multiplying effect to increase the discrimination. A minimum separation of disks of two inches was used to prevent interference in displacement patterns between the disks. This distance was originally chosen based on interpretation of the analogical results of Thum and Bautz(9). Analysis of the numerical results of this investigation verified that the distance was sufficient.

The original configuration of each of the nine specimens is given in Figure 16. The various diameters tested for each configuration is given in Table 1.

1. MATERIAL

The material specifications for the test specimens are:

MATERIAL	High strength aluminum conforming to A.S.T.M. Specification (24)
SIZE	2-1/8 inch diameter, 24 inches long
PROCESS	Cold Rolled
HEAT TREATMENT	Solution Heat-treated, stress relieved, artificially age-hardened per A.S.T.M. Specification T-651(25)

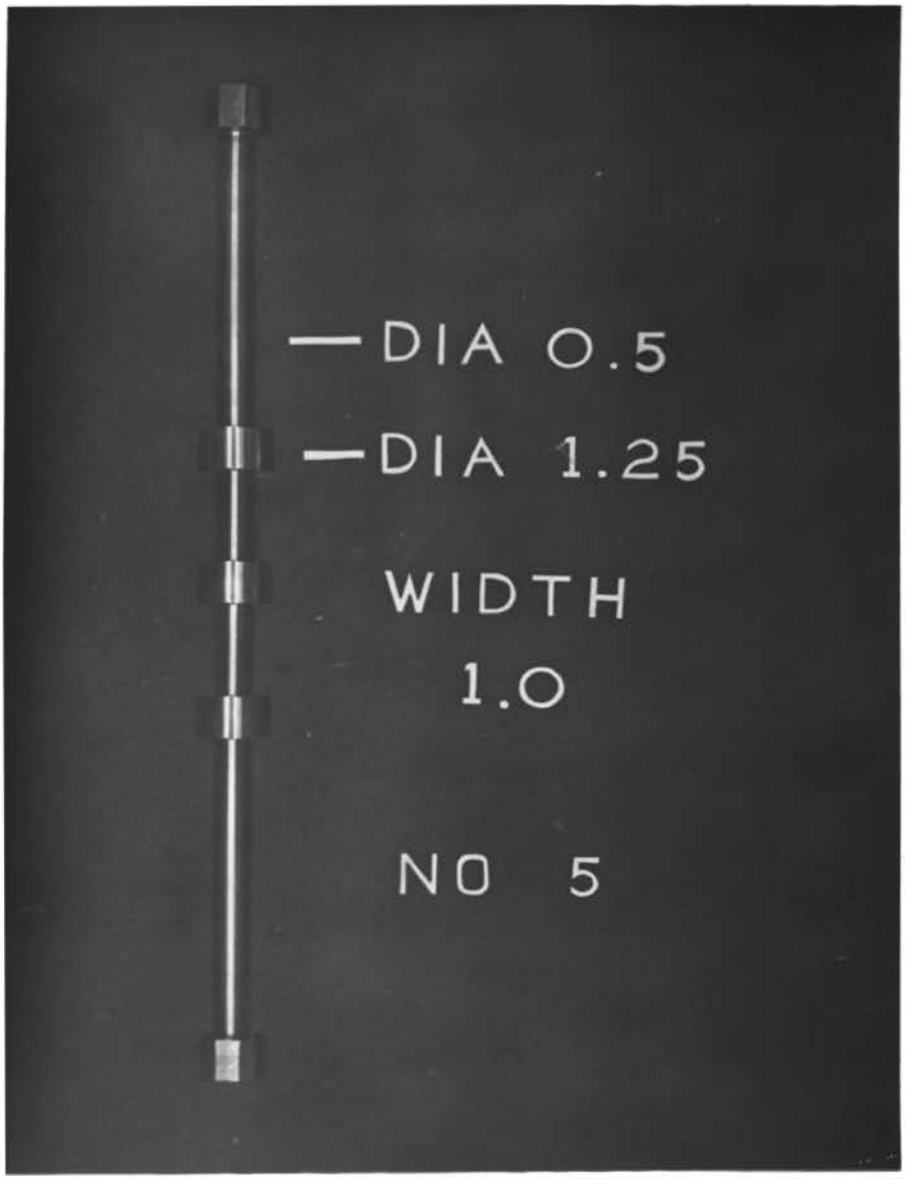

Figure 15. A Photograph of a Typical Test Specimen

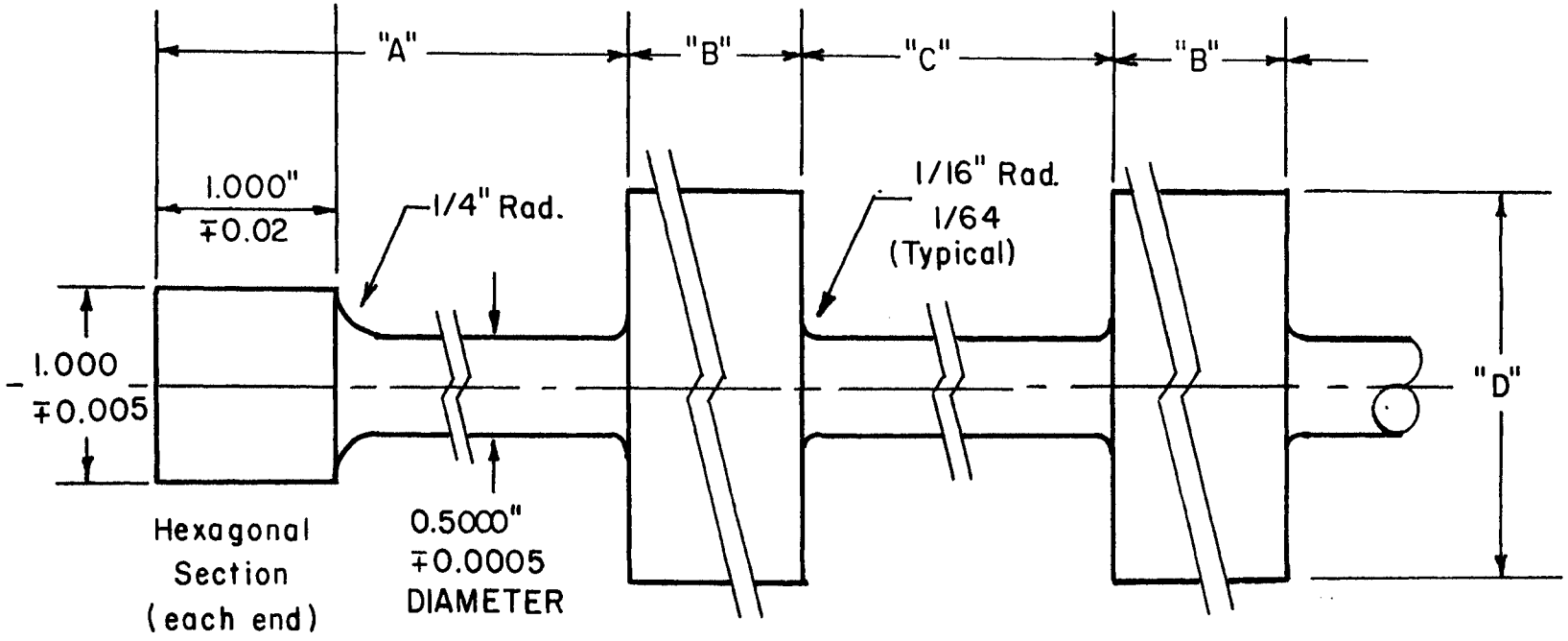

TOLERENCE

Dimension "A" - ∓0.010
" "B" - ∓0.0005
" "C" - ∓0.005
" "D" - ∓0.0005

NOTE : Lettered Dimensions are given in Table I.

Figure 16. Specification of Test Specimen Geometry

SPECIMEN NUMBER		DIMENSION SETS										
NUMBER	of DISKS	"A"	"B"	"C"	"D-1"	"D-2"	"D-3"	"D-4"	"D-5"	"D-6"	"D-7"	"D-8"
1	4	8.30	0.125	2.30	---	---	---	1.000	0.875	0.750	0.625	0.500*
2	4	8.20	0.250	2.20	---	1.500	1.250	1.000	0.875	0.750	0.625	0.500
3	4	8.00	0.500	2.00	2.000	1.500	1.250	1.000	0.875	0.750	0.625	0.500
4	3	8.44	0.750	2.44	2.000	1.500	1.250	1.000	0.875	0.750	0.625	0.500
5	3	8.25	1.000	2.25	2.000	1.500	1.250	1.000	0.875	0.750	0.625	0.500
6	2	9.00	1.500	3.00	2.000	1.500	1.250	1.000	0.875	0.750	0.625	0.500
7	2	8.00	2.000	2.00	2.000	1.500	1.250	1.000	0.875	0.750	0.625	0.500
8	2	8.00	3.000	2.00	2.000	1.500	1.250	1.000	0.875	0.750	0.625	0.500
9	1	9.50	5.000	--	2.000	1.500	1.250	1.000	0.875	0.750	0.625	0.500

*Disk Completely removed

Table I. Values for Test Specimen Configuration

The minimum properties given by the manufacturer (26) are:

YEILD POINT	73,000 pounds per square inch
ULTIMATE STRENGTH	83,000 pounds per square inch
SHEAR STRENGTH	48,000 pounds per square inch

The nominal values of material properties given by manufacturer:

MODULUS OF ELASTICITY	10.4×10^6 pounds per square inch
POISSON'S RATIO	0.33
MODULUS OF RIGIDITY OR SHEARING MODULAS OF ELASTICITY	3.9×10^6 pounds per square inch

E. TEST PROCEDURE

The test was conducted in three stages. The first stage consisted of the frame alignment, which was necessary only in the original equipment setup or when the equipment had been moved. The second stage was made up in two parts, the specimen mounting and the optical alignment. This second stage was necessary at the start of each test series. A test series constituted the complete testing of one specimen configuration. The third stage consisted of two parts, the load cell calibration and the test run. Implimentation of this third stage constituted a test segment. Three test segments made up the test series.

The first segment was made with increasing loads, the second with decreasing loads, and the third with increasing loads.

1. FRAME ALIGNMENT

The purpose of the frame alignment was to place the loading frame, displacement gage, and light source in the proper relative positions.

The first step was to adjust the loading frame and the displacement gage to a set distance and proper attitude. The displacement gage rail was leveled by adjusting the leveling nuts on each of the stands. A bubble type level was used as an indicator. Next, the loading frame was positioned along a line perpendicular to the displacement rail so that there was approximately 140 inches between the center position of the displacement gage(67.57 inches from the reference) and the center of a test specimen held in the loading frame. The special tape used for this measurement was attached to the test specimen and was used to measure the distance to the knife edge of the light beam scanner.

By adjusting the three floor contact points of the loading frame, the test specimen was placed in a vertical position. A check for perpendicularity between the loading frame and displacement gage was made by moving the displacement gage to secondary test positions at indicated

points of 2.57 inches and 132.57 inches. The distance to the loading frame from these locations should be 154.35 inches. Adjustments in the relative position was made by moving the loading frame. After each such adjustment, the vertical position of the test specimen was realigned and all three distances from the displacement gage to the test specimen were remeasured and the process repeated until the loading frame was in the proper position.

The second step was to align the light source along the perpendicular line from the displacement gage to the test specimen.

First, the height of the light source stand was set so that the source was slightly above the minimum height at the light scanner's knife edge. Then, the displacement gage was set at the center position and the light source was adjusted to the position where the back beam from the laser was centered on the knife edge and the forward beam was centered on the test specimen in the loading frame.

2. SPECIMEN MOUNTING

There were two steps to the mounting of the test specimen: the first was to install the specimen gage, and the second to mount the specimen and the gage in the loading frame.

The four parts of the gage were placed over the test

specimen with the movable attachment points loosened. Each of the two segments were joined with the case bolts. The position along the specimen was established where the lower attachment was to be made, and the gage moved along the specimen to this point. Then, the movable attachment point on the lower segment was tightened to about five inch-pounds torque. The attachment point of the upper unit remained loose.

Next, the upper end of the test specimen was mounted in the hexagonal socket of the upper loading frame unit and the socket clamped. The lower unit of the loading frame was moved up to engage the lower socket to the specimen. The socket was oriented so that the moment arm had the maximum movement possible. Before locking the lower unit to the frame, the lower unit was aligned to a vertical position with a bubble level.

Two major precautions were necessary during these operations: (1) movable attachment points were checked for sharpness before closing the specimen gage case, (2) care was taken not to touch or otherwise get foreign material on the mirrors of the specimen gage.

3. OPTICAL ALIGNMENT

There were two major points to be accomplished in the alignment of the optical system. First, the specimen gage mirrors must be set so that the reflected light beam was

within the range of the displacement gage. Second, the mounting of the specimen gage on the specimen was completed.

With the light source turned on, the vertical adjustment of the source was moved so that the light beam fell on the upper mirror of the gage. The upper segment of the gage was rotated until the reflected beam was near the reference position of the displacement gage. The upper segment was then locked to the specimen with approximately twenty inch-pounds of torque on the movable attachment point.

The light beam was then moved to the lower mirror by adjusting the light source, and the lower segment was loosened from the test specimen and rotated so that the reflected beam was near the reference position of the displacement gage. The special spacer was inserted between the two specimen gage segments, the lower segment was forced upward against the spacer, and then locked to the specimen with approximately twenty inch-pounds torque on the movable attachment points.

If the reflected beam from either mirror were too high or too low for the range of the displacement gage, slight vertical adjustments were made using the mounting screws of the mirrors on the specimen gage.

4. LOAD CELL CALIBRATION

Careful testing required frequent recalibration of

the load cell. The load cell required recalibration when it had not been in use for any appreciable length of time. Changes of calibration were due to temperature variations and to apparent internal creep inherent in the instrument.

It should be noted that both the load cell instrument and the readout required a warm-up period of at least twelve hours in order to reduce the temperature effects. Another precaution taken was to leave the load cell in a loaded condition only when it is required for test runs or calibration; this reduced the inherent creep.

Calibration of the load cell was accomplished with the cell in the calibration stand with the flat anvil in place. During calibration, as well as during test runs, particular precautions were taken to reduce the short term transients of the indicated zero point after loads were removed.

The calibration weight was loaded on the cell and allowed to set for five minutes. Then the load was removed, allowing the transients to die out. Then, after about one minute, the zero point was set on the transducer-amplifier unit using the digital readout. The calibration load was then imposed on the test cell and the transients again allowed to die out. The calibration was set on the instrument for the proper load reading on the digital read-out. This procedure was repeated several times until no further adjustments were necessary in either the zero point

or the calibration setting.

5. TEST RUN PROCEDURE

A test run could have been made in the direction of increasing or decreasing load, since the test run procedure was not altered except for the order of load settings. Each run consisted of ten data points, taken at evenly spaced load settings between 60 and 600 inch-pounds applied torque(indicated loads of 10 to 100 pounds). No test runs were made until at least one hour had elapsed since the completion of the previous test run.

The following procedure at each data point was used.

a. Set the load at approximately the desired setting, using the load instrumentation digital readout and the loading arm lead screw.
b. Release the load from the test cell by engaging the load lock-out cam on the load cell.
c. Allow the transients to die out of the load instrumentation(approximately one minute) and set the zero on the transducer-amplifier using the digital readout.
d. Release the load lock-out cam, again allowing the transients to die out, and set the load to the desired value.
e. Move the beam to the lower mirror on the specimen gage with the light source vertical adjustment.
f. Move the traveling platform of the displacement

gage to the reference point and set the dial indicator at zero.

g. Move the traveling platform to the vicinity of the laser beam. The platform was moved carefully so the dial gage did not slip.

h. Insert the alignment gage in the transducer holder on the platform, and move the platform until the laser beam splits the knife edge. Center the beam on the transducer holder by vertically adjusting the holder. Rotate the holder until the shadow of the knife edge falls on the reference point of the alignment gage. Lock the transducer holder in this position.

i. Replace the alignment gage with the power meter transducer, not letting the full laser beam fall on the transducer. Move the traveling table into the beam path in the direction of decreasing distance from the displacement reference to a power level of 0.25 milliwatts.

j. Record the distance from the reference point using the dial indicator on the traveling platform.

k. Adjust the light beam source to the upper mirror and repeat steps g thru j.

General precautions which were observed during the test run are: (1) not letting the laser beam impinge on the power meter except when setting the displacement gage,

(2) not making displacement gage settings when smoke or other airborne materials may diffuse the laser beam, (3) not allowing a load to remain on the test cell except where required for test run or calibration, (4) not allowing the test specimen to remain in the loaded state for an unnecessarily long period of time.

F. DISCUSSIONS OF ACCURACY

The experimental apparatus was constructed so that a high degree of accuracy was obtainable. The estimates of the accuracy of the various devices involved, are based on data taken in order to establish these limits. There were two major factors that established the accuracy.

One of the major factors affecting accuracy was the load on the specimen. The load was measured by the load cell and sensed by a null voltmeter. By using standard weights, it was established that this measurement system was accurate to approximately plus or minus one-tenth of a pound throughout the range used. This force acted on a six inch moment arm, giving a torque accurate to plus or minus six-tenths of an inch-pound. To interpret the effect of this error on the experimental values for specimen flexibility, which are in terms of the displacement in radians due to one inch-pound applied torque, the effect was evaluated at the median value of load. The median load was fifty pounds, producing three hundred inch-pounds of torque. The average load error was two-tenths percent.

The median value of the experimental result was 0.5 X 10^{-3} radians per inch-pound. Therefore, the effect on the results amounted to plus or minus 1.0 X 10^{-6} radians per inch-pound.

The second major measurement factor in the flexibility measurement was the angle of deflection. This angle was determined by measuring the lateral deflection of the laser beam. The lateral measurement error plus the error in offset detection of the laser was determined to be approximately two-hundredths of an inch. Taking into account the arm length and the double angle measurement, an error of approximately 7.0 X 10^{-4} radians was found. Translating this error to the effect on the experimental results when the average load was three hundred inch-pounds gave an error of approximately 2.0 X 10^{-7} radians per inch-pound.

A maximum total flexibility error of approximately 1.2 X 10^{-6} radians per inch-pound could result from the load and angular measurement errors.

G. TREATMENT OF EXPERIMENTAL DATA

The data taken was analyzed in two steps. The first step was to reduce the load and lateral distance information obtained in the test segment to values of applied torque on the test specimen and its angle of deflection. The second step was to reduce these measured values to the corresponding value for the flexibility of the test

specimen.

The load and lateral distance data was reduced to the applied torque and deflection values using relationships inherent in the design of the test equipment. The applied torque was the product of the load and moment arm of the frame. The relative angle of deflection between the mirrors of the specimen gage was determined by finding the angle each made with the reference line of the setup. The angle of mirror was determined from the geometric relationships of the setup.

Next, the applied torque and deflection information was reduced from each test segment to a value for the flexibility of the shaft configuration. The results of each test segment was subjected to a least squares fit using a first degree curve for the ten data points. When all three runs were completed, the data from all three test segments were lumped together and subjected to a least squares fit. This value was then taken as the experimental value of flexibility. The value was the slope of the curve representing the deflection in radians as a function of the load in inch-pounds.

The least squares fit used was a polynomial regression limited to first degree with the equations being solved using the Gauss-Jordan technique. The fit of the curve was forced on the applied torque variable because the error in this variable was approximately five times the

error in the angle of deflection.

The experimental test results are given for each specimen so that the results were grouped on the same number of disks and width of disk, but with various disk diameters. The results are listed in APPENDIX E.

CHAPTER V

RESULTS AND CONCLUSIONS

A. PRESENTATION OF RESULTS

The flexibility determined from the numerical and experimental evaluations are for a shaft-disk geometry which includes the effects of the disk and a portion of the basic shaft. In order to find the effect of the disk alone, it was necessary to subtract the effect of the basic shaft. The flexibility contribution of the basic shaft was evaluated using the classical formula for deflection of a cylindrical shaft in torsion. This form then lumps all the effects of the diameter change into the disk flexibility. The flexibilities of the disk portion are given in Figures 17 to 25. For comparative purposes, the value of the flexibility of the disk using the classical formulation for a cylindrical shaft is also shown. It is this value which is frequently used at present for flexibility calculations for disks.

The graphs of flexibility show that there is a limit beyond which an increase in the disk diameter does not effect its flexibility. This indicates that some material in the disk was ineffectual in resisting deflection and that this material was in a very low state of stress. The finite element calculations indicated that a low stress existed in the disk section near the diameter change.

The area of low stress extended back into the disk further as the distance along a radius line increased beyond the radius of the basic shaft. This same effect was observed in a model shown in Figure 26 of a disk in which the material outside a line from the fillets outward was arbitrarily declared ineffectual in resisting twist, while that inside was declared fully effective and the angle of twist evaluated using the general form of the equation for twist. This equation is

$$\phi = \int_Z \frac{T\,dz}{J\,G} \qquad (5.1)$$

where ϕ is the angle of twist, T is the applied torque, z is length, Z is a generator over the length, G is the shearing modulus of elasticity, and J is the polar moment of inertia and is a function of the length z.

Using the idea of the ineffectual material, the flexibility of the disk for various angles of the line to the axis of symmetry were evaluated, and the angle which gave the best approximation for all geometries was chosen. This angle was found to be approximately fifty-five degrees. The flexibilities using this approximation are also shown in Figures 17 to 25.

B. CONCLUSIONS

The integral disk on a shaft does not present the resistance to torsional deflection that the use of

elementary shaft theory predicts. The flexibility instead reaches a lower bound as the diameter of the disk is increased, which is dependent on the width of the disk. An approximation of the flexibility of the disk can be found by the use of an arbitrary model which excludes a portion of the disk as ineffective in resisting torsion.

A finite element method has been presented for obtaining a numerical stress analysis of a general axisymmetric solid. It has been demonstrated that this method is capable of calculating displacements due to torsion with an acceptable degree of accuracy.

Further extensions of the investigation would be of considerable interest in two directions: first, to investigate the effect of shaft diameter on the proposed approximation as well as to find the effect of the material properties on the angle of the arbitrary cut-off line, second, to more fully develop the finite element method.

The extensions to the proposed finite element method can be itemized as follows:

(i) Optimization of numerical calculations

(ii) Verification of numerically calculated stresses for the various types of loading

(iii) Extension of the method to include nonlinear material properties.

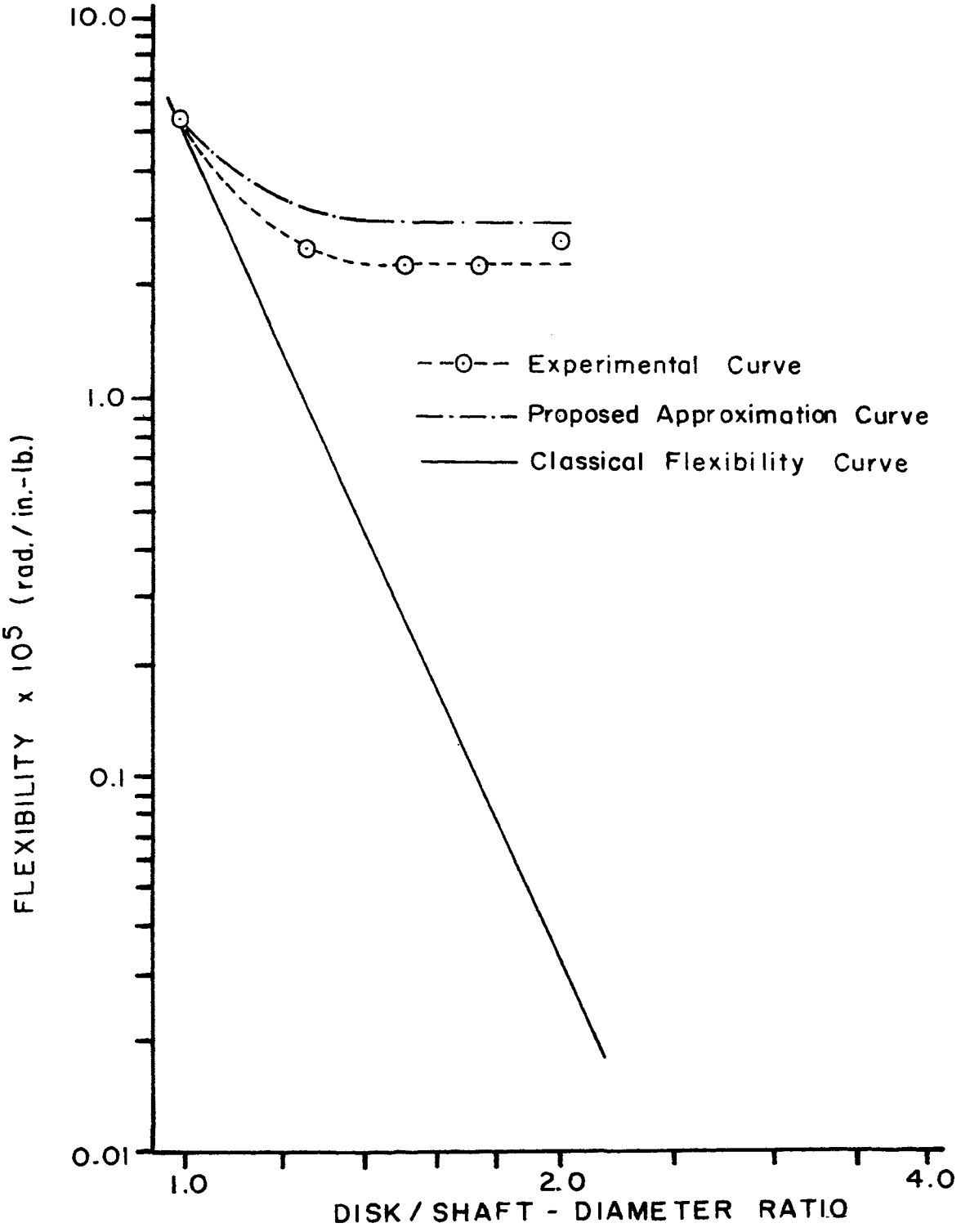

Figure 17. Disk Flexibility -- Specimen Number 1, Disk Width, 0.125 inches; Shaft Diameter - 0.5 Inches

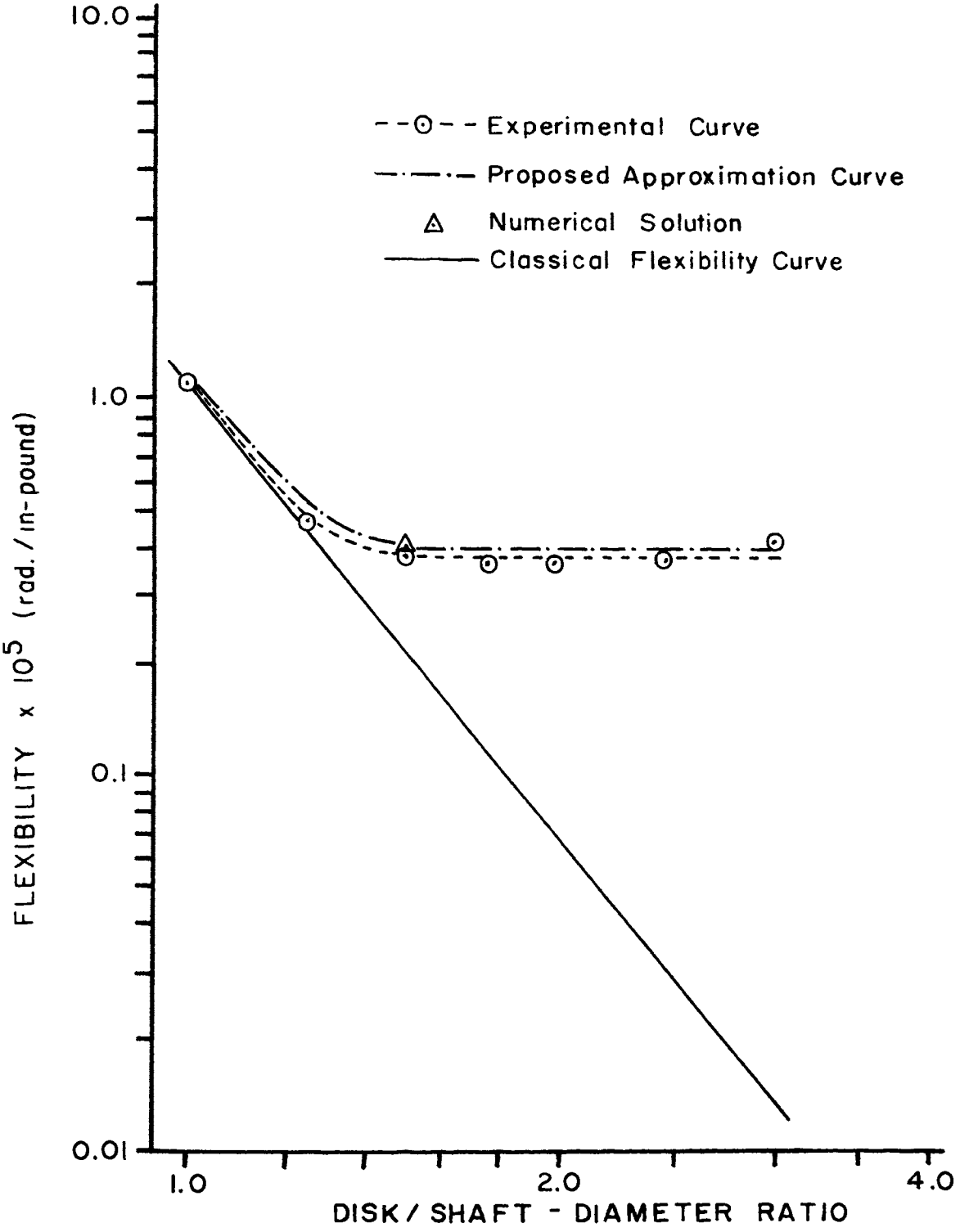

Figure 18. Disk Flexibility -- Specimen Number 2, Disk Width, 0.25 Inches; Shaft Diameter - 0.5 Inches

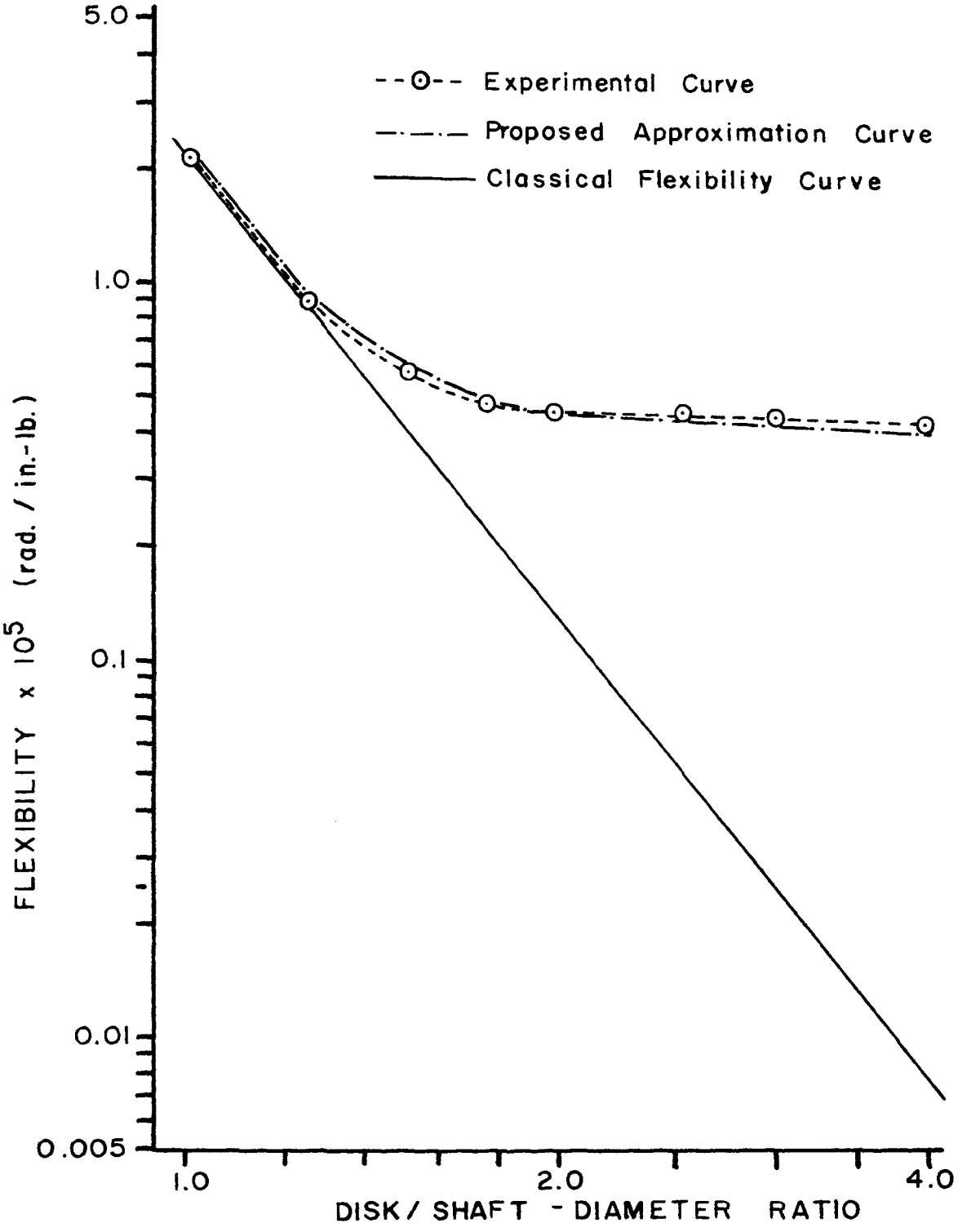

Figure 19. Disk Flexibility -- Specimen Number 3, Disk Width, 0.50 Inches; Shaft Diameter - 0.5 Inches

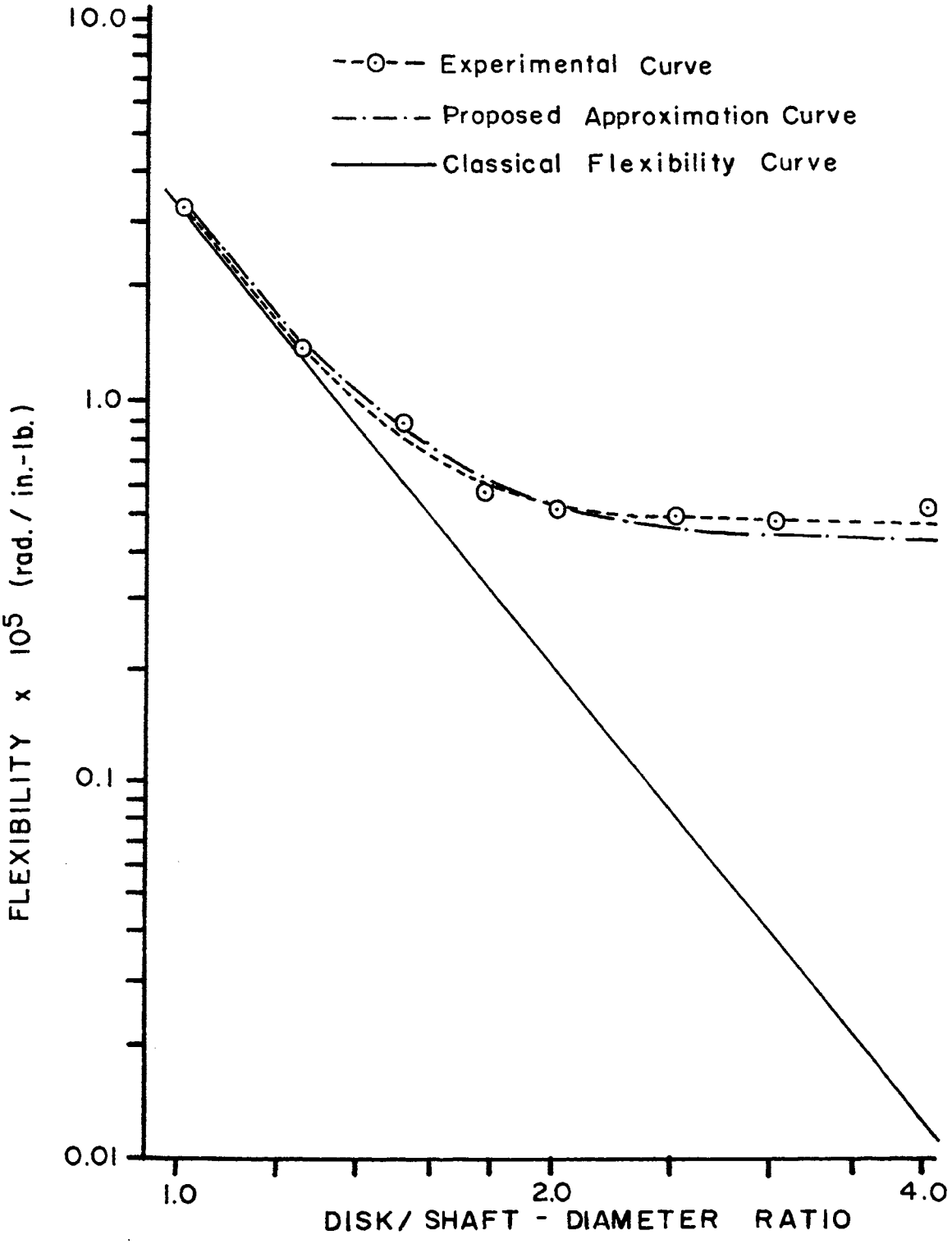

Figure 20. Disk Flexibility -- Specimen Number 4, Disk Width, 0.75 Inches; Shaft Diameter - 0.5 Inches

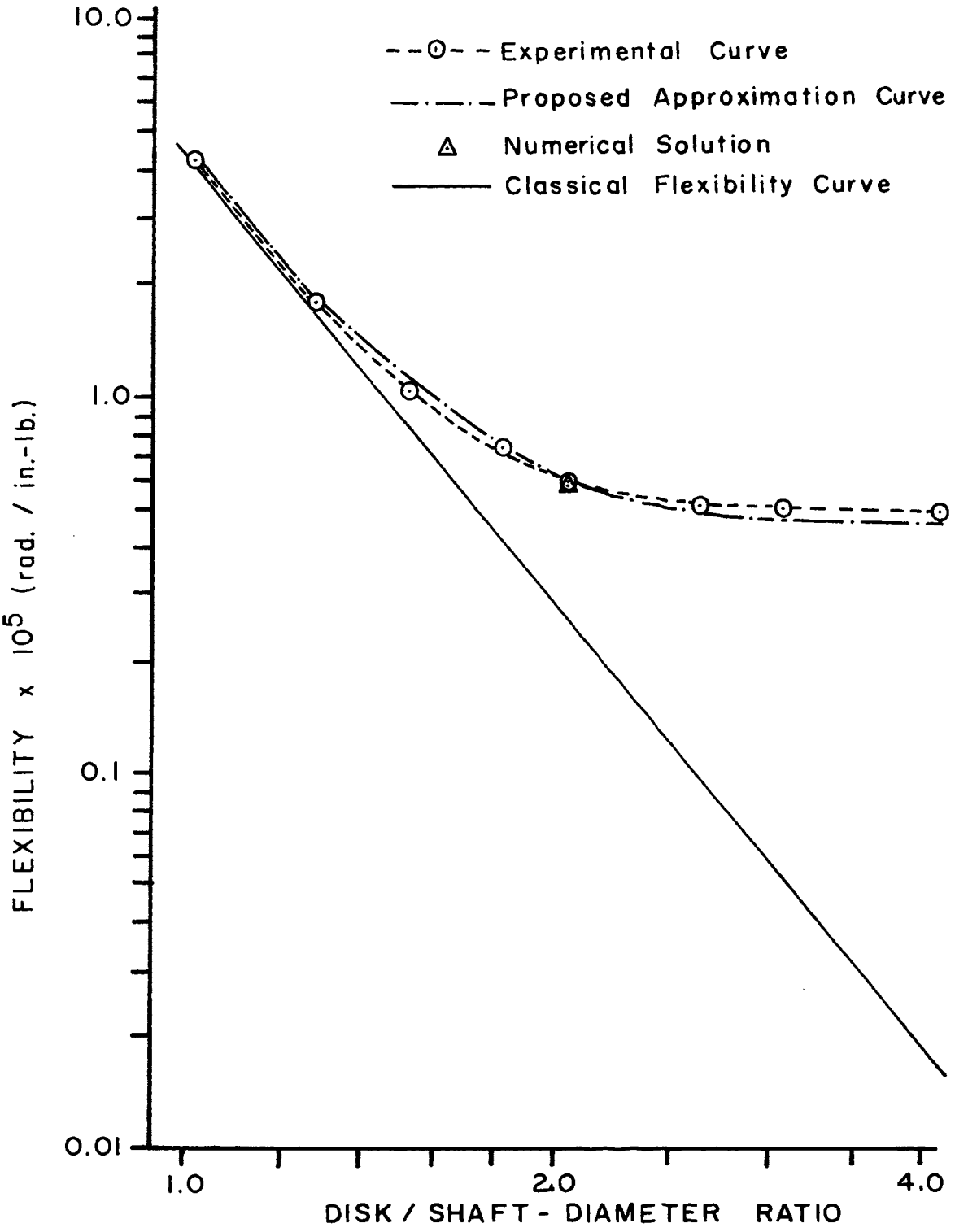

Figure 21. Disk Flexibility -- Specimen Number 5, Disk Width, 1.00 Inches; Shaft Diameter - 0.5 Inches

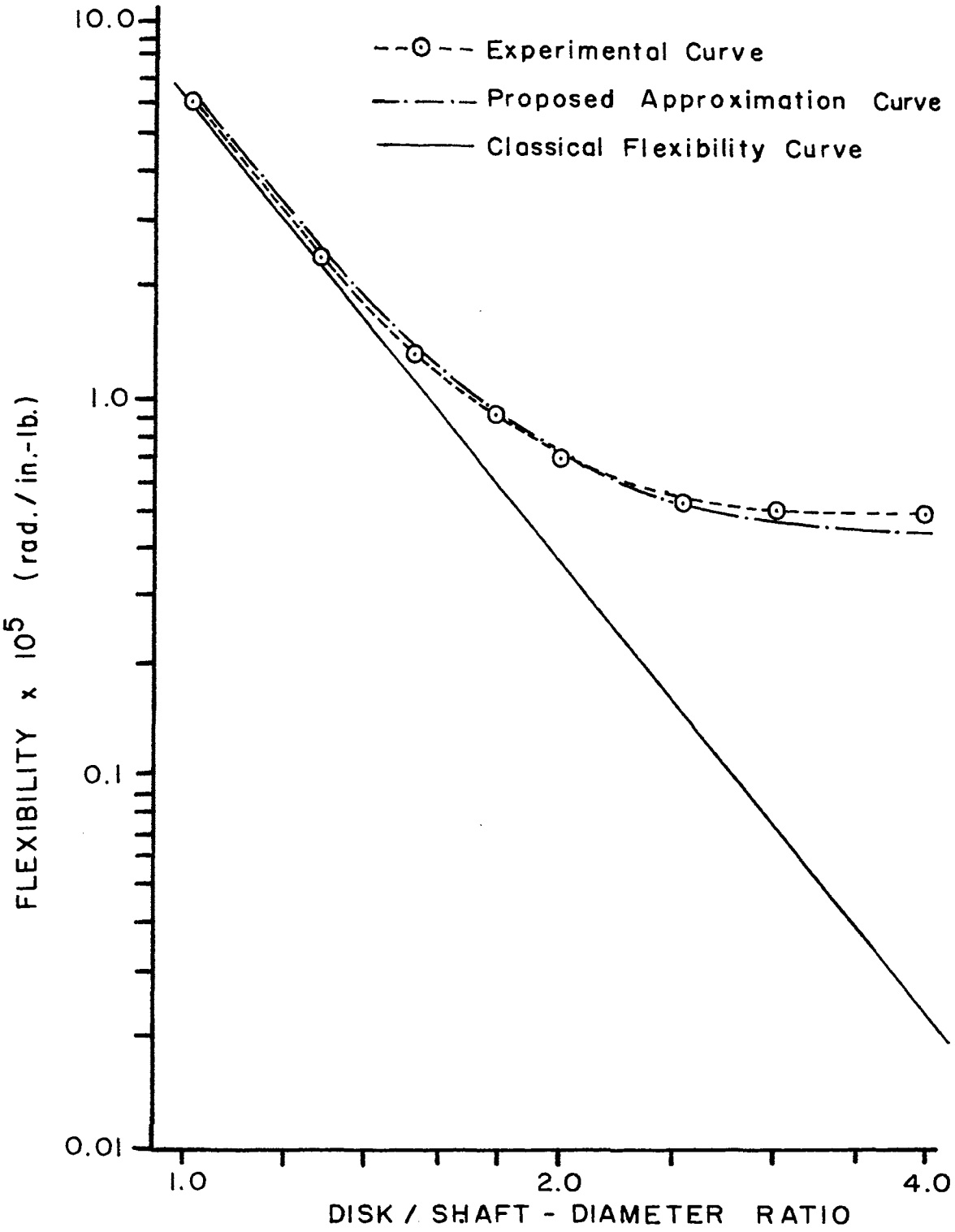

Figure 22. Disk Flexibility -- Specimen Number 6, Disk Width, 1.50 Inches; Shaft Diameter - 0.5 Inches

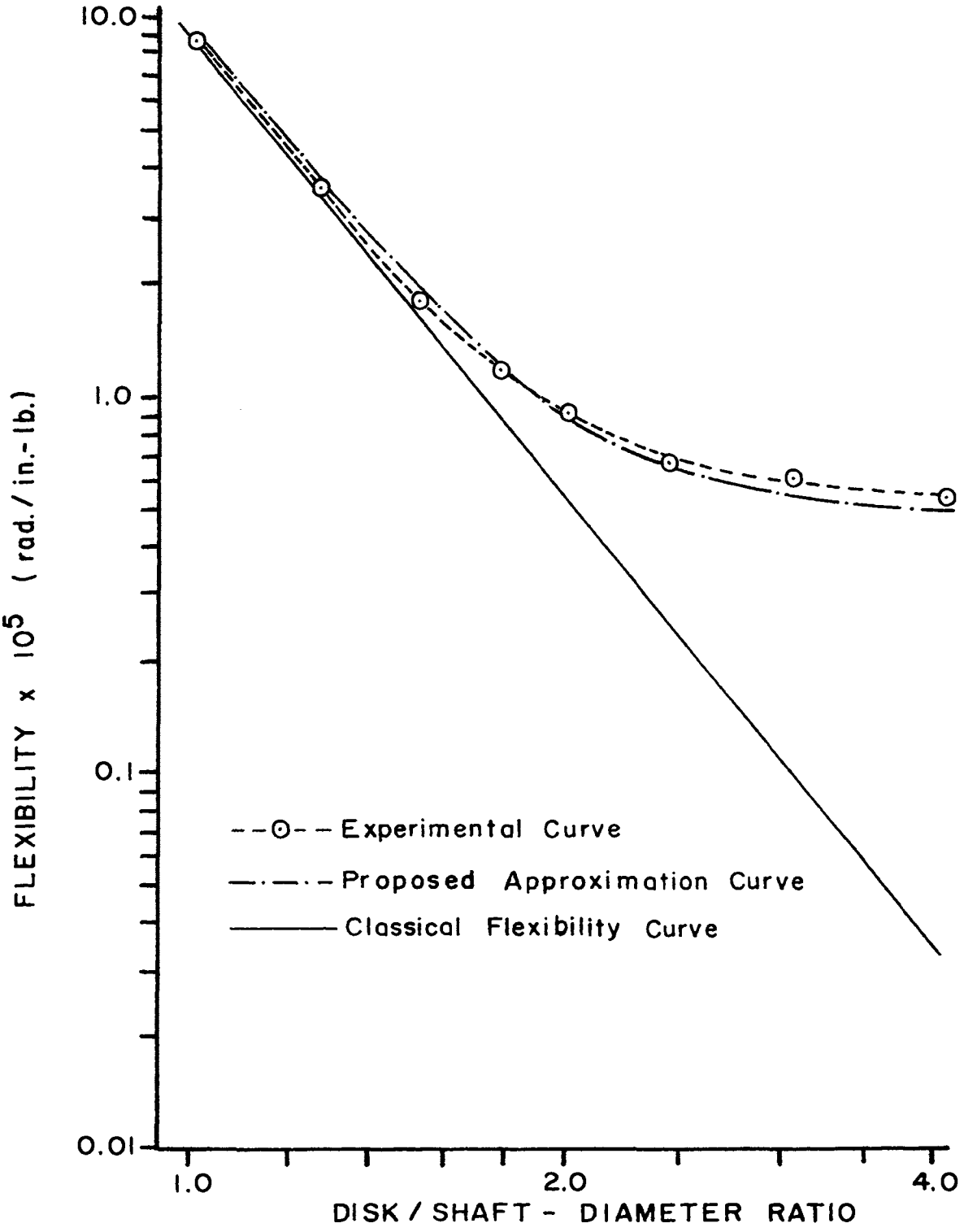

Figure 23. Disk Flexibility -- Specimen Number 7, Disk Width, 2.0 Inches; Shaft Diameter - 0.5 Inches

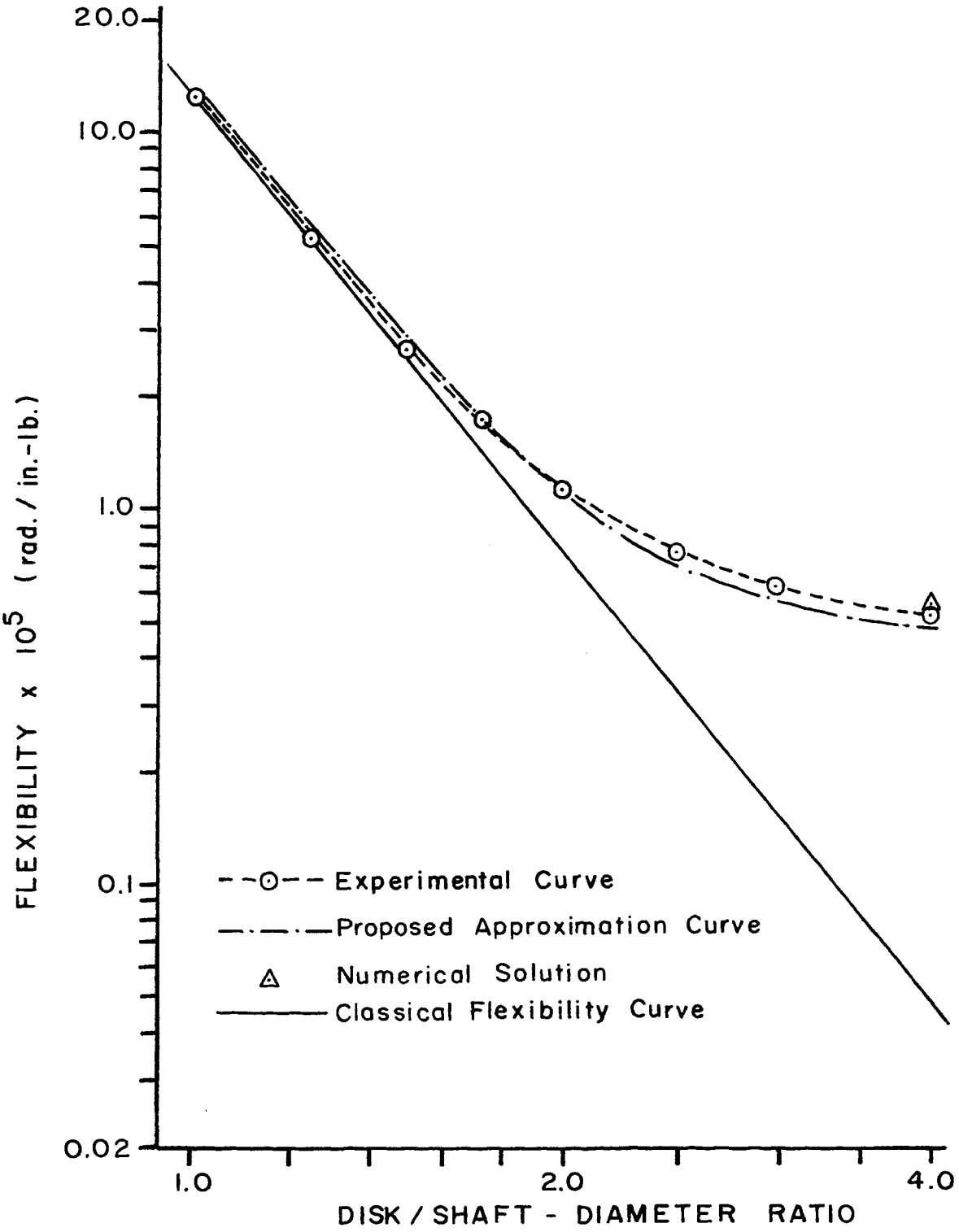

Figure 24. Disk Flexibility -- Specimen Number 8, Disk Width, 3.0 Inches; Shaft Diameter - 0.5 Inches

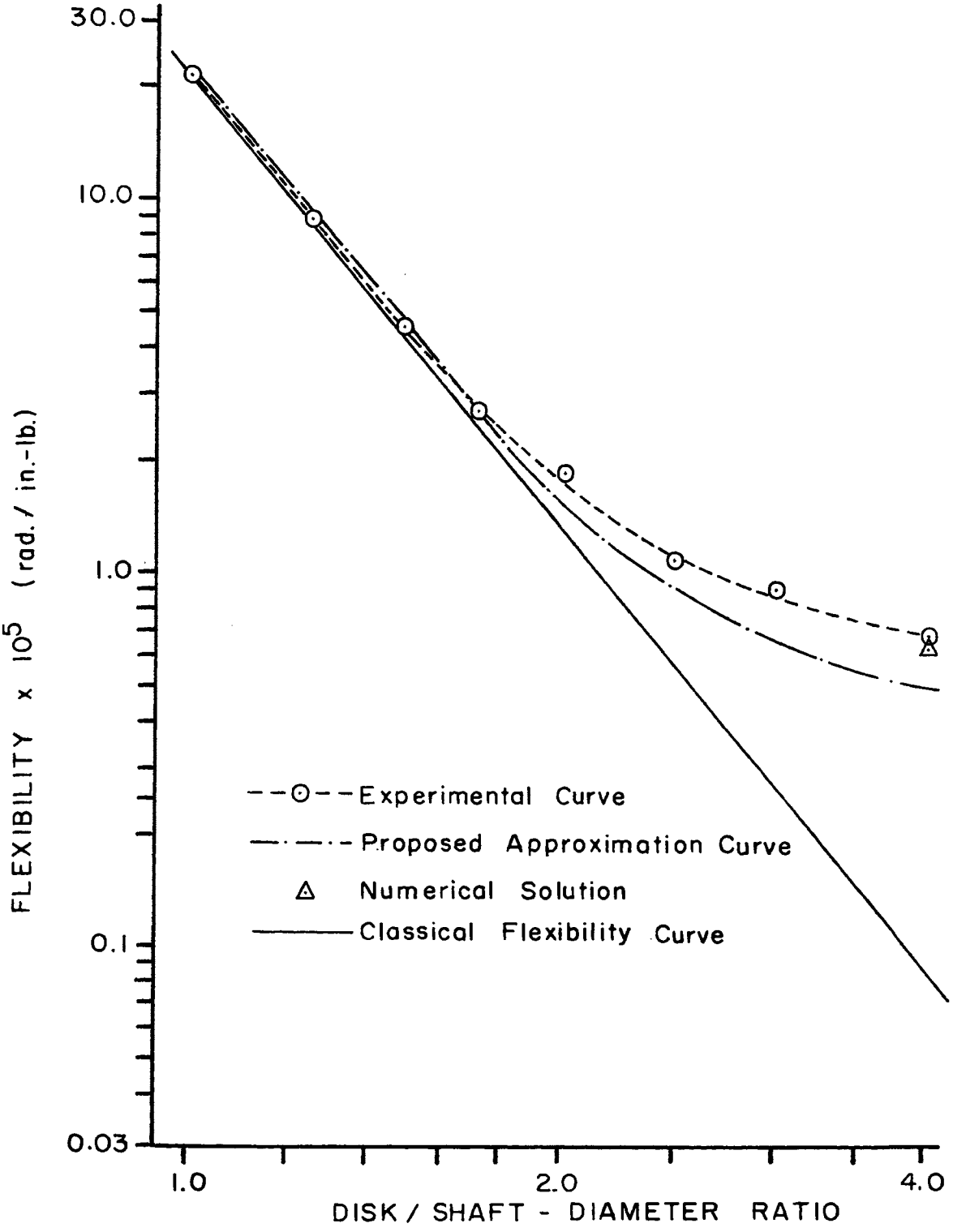

Figure 25. Disk Flexibility -- Specimen Number 9, Disk Width, 5.0 Inches; Shaft Diameter - 0.5 Inches

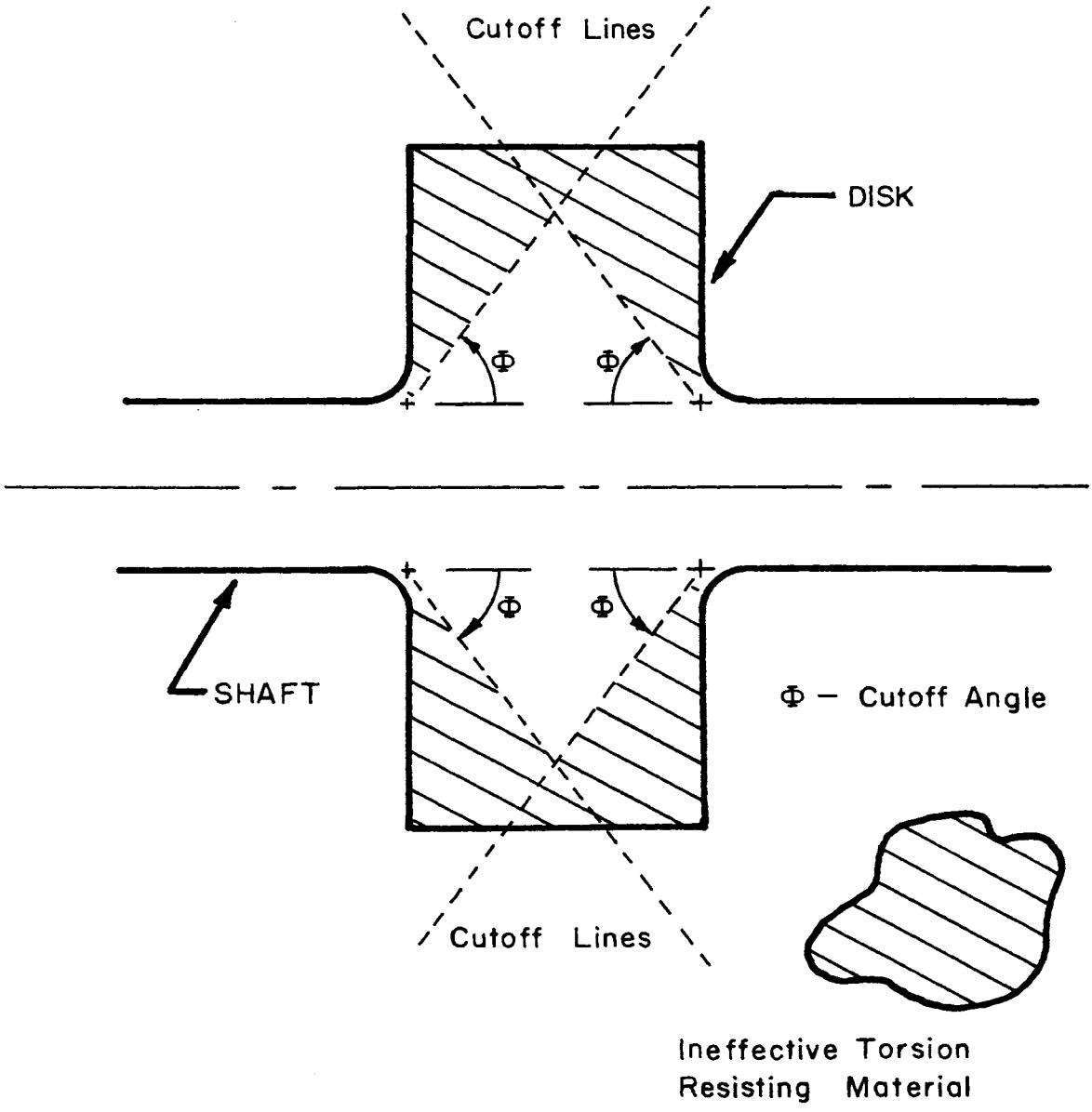

Figure 26. Proposed Torsion Loaded Shaft Model

APPENDIX A

FORMULATION OF THE INVERSION OF THE NODAL COORDINATE MATRIX

The inversion of the nodal coordinate matrix $[C^e]$ is carried out in the form of the inverse of a submatrix and then the complete inverse nodal coordinate matrix $[C^e]^{-1}$ is reconstructed from this. The defining equation for the nodal coordinate matrix $[C^e]$ is given by Equation (3.8) as

$$\{\delta^e\} = [C^e]\{\alpha^e\} \tag{A-1}$$

It is shown in Equation (3.7) that the nodal coordinate matrix $[C^e]$ can be written in terms of the coordinate matrices $[P_i^e]$ evaluated at the node coordinates. For use in the inversion, it is useful to expand the coordinate matrix $[P_i^e]$* evaluated at the i-th node so that

$$[P_i] = \begin{bmatrix} \tilde{P}_i & \tilde{0} & \tilde{0} \\ \tilde{0} & \tilde{P}_i & \tilde{0} \\ \tilde{0} & \tilde{0} & \tilde{P}_i \end{bmatrix} \tag{A-2}$$

where

$$[P_i] = [1 \quad r_i \quad z_i \quad r_i^2 \quad r_i z_i \quad z_i^2] \tag{A-2a}$$

and

---

*The superscript ^{e} has been omitted throughout the remainder of this discussion.

$$[\tilde{0}] = [0 \quad 0 \quad 0 \quad 0 \quad 0 \quad 0] \tag{A-2b}$$

With this form defined, Equation (A-1) is now written as

$$\begin{Bmatrix} u_1 \\ v_1 \\ w_1 \\ u_2 \\ \cdot \\ \cdot \\ \cdot \\ w_6 \end{Bmatrix} = \begin{bmatrix} \tilde{P}_1 & \tilde{0} & \tilde{0} \\ \tilde{0} & \tilde{P}_1 & \tilde{0} \\ \tilde{0} & \tilde{0} & \tilde{P}_1 \\ \tilde{P}_2 & \tilde{0} & \tilde{0} \\ \cdot & \cdot & \cdot \\ \cdot & \cdot & \cdot \\ \cdot & \cdot & \cdot \\ \tilde{0} & \tilde{0} & \tilde{P}_6 \end{bmatrix} \begin{Bmatrix} \alpha_1 \\ \alpha_2 \\ \alpha_3 \\ \alpha_4 \\ \cdot \\ \cdot \\ \cdot \\ \alpha_{18} \end{Bmatrix} \tag{A-3}$$

From this expression, the equation for the radial displacement u is written as

$$\begin{Bmatrix} u_1 \\ u_2 \\ u_3 \\ u_4 \\ u_5 \\ u_6 \end{Bmatrix} = \begin{bmatrix} \tilde{P}_1 \\ \tilde{P}_2 \\ \tilde{P}_3 \\ \tilde{P}_4 \\ \tilde{P}_5 \\ \tilde{P}_6 \end{bmatrix} \begin{Bmatrix} \alpha_1 \\ \alpha_2 \\ \alpha_3 \\ \alpha_4 \\ \alpha_5 \\ \alpha_6 \end{Bmatrix} \tag{A-4}$$

and a submatrix of the nodal coordinate matrix $[\tilde{C}]$ is defined by

$$[u_i] = [\tilde{C}]\{\alpha_1 \quad \alpha_2 \quad . \quad . \quad . \quad \alpha_6\}^T \qquad \text{(A-5a)}$$

Similarly, the relationships for the angular and longitudinal displacements become

$$[v_i] = [\tilde{C}]\{\alpha_7 \quad \alpha_8 \quad . \quad . \quad . \quad \alpha_{12}\}^T \qquad \text{(A-5b)}$$

$$[w_i] = [\tilde{C}]\{\alpha_{13} \quad \alpha_{14} \quad . \quad . \quad . \quad \alpha_{18}\}^T \qquad \text{(A-5c)}$$

where the submatrix is

$$[\tilde{C}] = \begin{bmatrix} 1 & r_1 & z_1 & r_1^2 & r_1 z_1 & z_1^2 \\ 1 & r_2 & z_2 & r_2^2 & r_2 z_2 & z_2^2 \\ . & . & . & . & . & . \\ . & . & . & . & . & . \\ . & . & . & . & . & . \\ 1 & . & . & . & . & z_6^2 \end{bmatrix} \qquad \text{(A-6)}$$

Only this submatrix $[\tilde{C}]$ need be inverted, as it is identical for all three displacements. This procedure does require, however, the reconstruction of the whole inverse nodal coordinate matrix $[\tilde{C}]^{-1}$ on an element by element basis to obtain the proper form.

The inversion of the submatrix $[\tilde{C}]$ is carried out in a local coordinate system, where one axis of the local system coincides with one boundary of the element as shown in Figure 28. This arrangement gives the inverse of the

submatrix $[\tilde{C}]$ in a local coordinate form denoted as $[\tilde{C}']$.* By taking advantage of all the geometric relationships, the inverse is evaluated in a closed form. The inverse may be written with the non-zero elements given as h, as

$$[\tilde{C}']^{-1} = \begin{bmatrix} 1 & 0 & 0 & 0 & 0 & 0 \\ h_{21} & h_{22} & h_{23} & 0 & 0 & 0 \\ h_{31} & h_{32} & h_{33} & h_{34} & h_{35} & h_{36} \\ h_{41} & h_{42} & h_{43} & 0 & 0 & 0 \\ h_{51} & h_{52} & h_{53} & h_{54} & 0 & h_{56} \\ h_{61} & h_{62} & h_{63} & h_{64} & h_{65} & h_{66} \end{bmatrix} \tag{A-7}$$

To transform the inverse submatrix $[\tilde{C}']^{-1}$ into the global coordinates, it is multiplied by the transformation matrix $[\tilde{T}]$ defined in Appendix B. Thus

$$[\tilde{C}]^{-1} = [\tilde{T}][\tilde{C}']^{-1} \tag{A-8}$$

The elements of the inverse matrix $[\tilde{C}]^{-1}$ are placed in the proper element positions within the inverse nodal displacement matrix $[C]^{-1}$ according to the defining Equation (3.9). If the elements of the inverse submatrix $[\tilde{C}]^{-1}$ in global coordinates are denoted as C_{ij}, the form of the inverse nodal displacement matrix is shown as

---

*The prime (') indicates a quanity associated with the local coordinate system.

$$
[C]^{-1} = \begin{bmatrix}
C_{11} & 0 & 0 & C_{12} & 0 & 0 & C_{13} & 0 & 0 & C_{14} & 0 & 0 & C_{15} & 0 & 0 & C_{16} & 0 & 0 \\
C_{21} & 0 & 0 & C_{22} & 0 & 0 & C_{23} & 0 & 0 & C_{24} & 0 & 0 & C_{25} & 0 & 0 & C_{26} & 0 & 0 \\
C_{31} & 0 & 0 & C_{32} & 0 & 0 & C_{33} & 0 & 0 & C_{34} & 0 & 0 & C_{35} & 0 & 0 & C_{36} & 0 & 0 \\
C_{41} & 0 & 0 & C_{42} & 0 & 0 & C_{43} & 0 & 0 & C_{44} & 0 & 0 & C_{45} & 0 & 0 & C_{46} & 0 & 0 \\
C_{51} & 0 & 0 & C_{52} & 0 & 0 & C_{53} & 0 & 0 & C_{54} & 0 & 0 & C_{55} & 0 & 0 & C_{56} & 0 & 0 \\
C_{61} & 0 & 0 & C_{62} & 0 & 0 & C_{63} & 0 & 0 & C_{64} & 0 & 0 & C_{65} & 0 & 0 & C_{66} & 0 & 0 \\
0 & C_{11} & 0 & 0 & C_{12} & 0 & 0 & C_{13} & 0 & 0 & C_{14} & 0 & 0 & C_{15} & 0 & 0 & C_{16} & 0 \\
0 & C_{21} & 0 & 0 & C_{22} & 0 & 0 & C_{23} & 0 & 0 & C_{24} & 0 & 0 & C_{25} & 0 & 0 & C_{26} & 0 \\
0 & C_{31} & 0 & 0 & C_{32} & 0 & 0 & C_{33} & 0 & 0 & C_{34} & 0 & 0 & C_{35} & 0 & 0 & C_{36} & 0 \\
0 & C_{41} & 0 & 0 & C_{42} & 0 & 0 & C_{43} & 0 & 0 & C_{44} & 0 & 0 & C_{45} & 0 & 0 & C_{46} & 0 \\
0 & C_{51} & 0 & 0 & C_{52} & 0 & 0 & C_{53} & 0 & 0 & C_{54} & 0 & 0 & C_{55} & 0 & 0 & C_{56} & 0 \\
0 & C_{61} & 0 & 0 & C_{62} & 0 & 0 & C_{63} & 0 & 0 & C_{64} & 0 & 0 & C_{65} & 0 & 0 & C_{66} & 0 \\
0 & 0 & C_{11} & 0 & 0 & C_{12} & 0 & 0 & C_{13} & 0 & 0 & C_{14} & 0 & 0 & C_{15} & 0 & 0 & C_{16} \\
0 & 0 & C_{21} & 0 & 0 & C_{22} & 0 & 0 & C_{23} & 0 & 0 & C_{24} & 0 & 0 & C_{25} & 0 & 0 & C_{26} \\
0 & 0 & C_{31} & 0 & 0 & C_{32} & 0 & 0 & C_{33} & 0 & 0 & C_{34} & 0 & 0 & C_{35} & 0 & 0 & C_{36} \\
0 & 0 & C_{41} & 0 & 0 & C_{42} & 0 & 0 & C_{43} & 0 & 0 & C_{44} & 0 & 0 & C_{45} & 0 & 0 & C_{46} \\
0 & 0 & C_{51} & 0 & 0 & C_{52} & 0 & 0 & C_{53} & 0 & 0 & C_{54} & 0 & 0 & C_{55} & 0 & 0 & C_{56} \\
0 & 0 & C_{61} & 0 & 0 & C_{62} & 0 & 0 & C_{63} & 0 & 0 & C_{64} & 0 & 0 & C_{65} & 0 & 0 & C_{66}
\end{bmatrix} \qquad \text{(A-9)}
$$

APPENDIX B

DERIVATION OF TRANSFORMATION MATRIX

The transformation matrix $[\tilde{T}^e]$ is formed between the local and global coordinate systems such that

$$[\tilde{C}^e]^{-1} = [\tilde{T}^e][\tilde{C}^{e\prime}]^{-1} \tag{B-1}$$

The approach is to look at the displacement field to find the proper relationships. The local displacement field must be transformable to agree with the global displacement field. The equations for these are

$$\{f^e\} = [P^e][C^e]^{-1}\{\delta^e\} \tag{B-2a}$$

$$\{f^{e\prime}\} = [P^{e\prime}][C^{e\prime}]^{-1}\{\delta^{e\prime}\}* \tag{B-2b}$$

Relationships must exist between the global displacement field $\{f\}$ and the local displacement field $\{f'\}$ and also between the global nodal displacement $\{\delta\}$ and the local nodal displacement $\{\delta'\}$ since these are just displacements in different coordinate systems. Thus the field in the local system may be written in the global system and compared with the original global field. Any difference will then be the transformation matrix, such that

$$\{f\} = [P][C]^{-1}\{\delta\} = [P'][T][C']^{-1}\{\delta'\} \tag{B-3}$$

---

*The superscript ^{e} has been omitted throughout the remainder of this discussion.

The coordinate matrix $[P]$ may be written in expanded form as

$$[P] = \begin{bmatrix} \tilde{P} & \tilde{0} & \tilde{0} \\ \tilde{0} & \tilde{P} & \tilde{0} \\ \tilde{0} & \tilde{0} & \tilde{P} \end{bmatrix} \tag{B-4}$$

And the nodal displacements may be written as u_i, v_i, and w_i. Then the displacement field is written as

$$\begin{aligned} u &= [\tilde{P}][\tilde{C}]^{-1} u_i \\ v &= [\tilde{P}][\tilde{C}]^{-1} v_i \\ w &= [\tilde{P}][\tilde{C}]^{-1} w_i \end{aligned} \tag{B-5}$$

This displacement field may also be written in the primed coordinate system so that

$$\begin{aligned} u' &= [\tilde{P}'][\tilde{C}']^{-1} u_i' \\ v' &= [\tilde{P}'][\tilde{C}']^{-1} v_i' \\ w' &= [\tilde{P}'][\tilde{C}']^{-1} w_i' \end{aligned} \tag{B-6}$$

The following relationships exist between the primed and unprimed displacements

$$u = u' \cos\beta + w' \sin\beta$$

$$v = v'$$

$$w = u' \sin\beta + w' \cos\beta \qquad \text{(B-7)}$$

$$u' = u \cos\beta + w \sin\beta$$

$$v' = v$$

$$w' = -u \sin\beta + w \cos\beta$$

Evaluating u in terms of the local system, this becomes

$$u = [P'][C']^{-1}(u_i \cos\beta + w_i \sin\beta)\cos\beta - [P'][C']^{-1} (-u_i \sin\beta + w_i \cos\beta)\sin\beta \qquad \text{(B-8)}$$

or

$$u \quad [P'][C']^{-1}\left(u_i(\cos^2\beta + \sin^2\beta) + w_i(\sin\beta\cos\beta - \cos\beta\sin\beta)\right) \qquad \text{(B-8a)}$$

Therefore, when this is repeated for v and w it is found that

$$u = [P'][C']^{-1} u_i$$

$$v = [P'][C']^{-1} v_i \qquad \text{(B-9)}$$

$$w = [P'][C']^{-1} w_i$$

comparing this equation with Equation (B-5), it is seen that

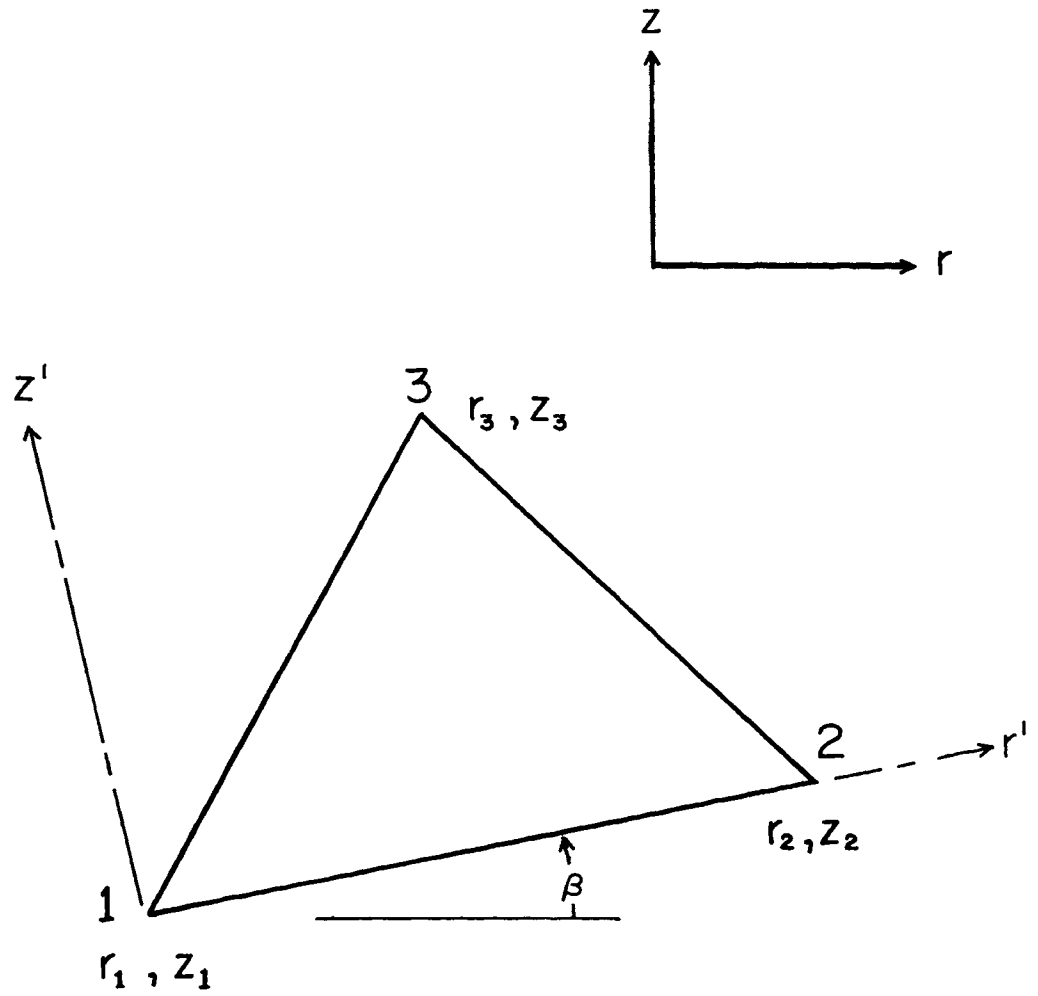

Figure 27. Triangular Element With Local and Global Coordinate Frames

$$[\tilde{P}'][\tilde{C}']^{-1} = [\tilde{P}][\tilde{C}]^{-1} \tag{B-10}$$

Substituting the desired transformation from Equation (B-1) in this equation, it becomes

$$[\tilde{P}'][\tilde{C}']^{-1} = [\tilde{P}][\tilde{T}][\tilde{C}']^{-1} \tag{B-11}$$

or

$$[\tilde{P}'] = [\tilde{P}][\tilde{T}] \tag{B-11a}$$

which explicitly defines the transformation matrix $[\tilde{T}]$.

In expanded form, this equation becomes

$$\begin{bmatrix} 1 & r' & z' & r'^2 & r'z' & z'^2 \end{bmatrix} = \begin{bmatrix} 1 & r & z & r^2 & rz & z^2 \end{bmatrix}[\tilde{T}] \tag{B-12}$$

The geometric relationships between the local and global coordinates are

$$\begin{aligned} r' &= (r-r_1)\cos\beta + (z-z_1)\sin\beta \\ z' &= -(r-r_1)\sin\beta + (z-z_1)\cos\beta \\ r &= r_1 + r'\cos\beta - z'\sin\beta \\ z &= z_1 + r'\sin\beta + z'\cos\beta \end{aligned} \tag{B-13}$$

Substituting Equation (B-13) into Equation (B-12) defines the transformation matrix $[\tilde{T}]$.

APPENDIX C

AREA INTEGRALS

The integrals which are evaluated have a number of functions which must be integrated over the element area. The list includes powers of r from the minus one power to the fifth power, powers of z from the first to the fourth, and various cross product terms of r and z. In order to assist in the evaluation of these integrals, a general approach is used.

A total area integral for the element is evaluated by breaking it up into three sub-area integrals, I_1, I_2, and I_3, shown in Figure 28 and evaluating each separately. Then the total integral I is

$$I = I_1 + I_2 - I_3 \qquad \text{(C-1)}$$

Each sub-integral is evaluated in a similar manner. The line boundary of integration formed by the element boundary is written in the form

$$z = \eta_1 + \eta_2 r$$

so that the limits of integration in the longitudinal z-direction are from zero to the line boundary. The integral limits in the radial r-direction are the r-coordinates of the nodes of the line boundary.

This is repeated for each sub-integral, and the total integral is then evaluated. This same procedure is used for

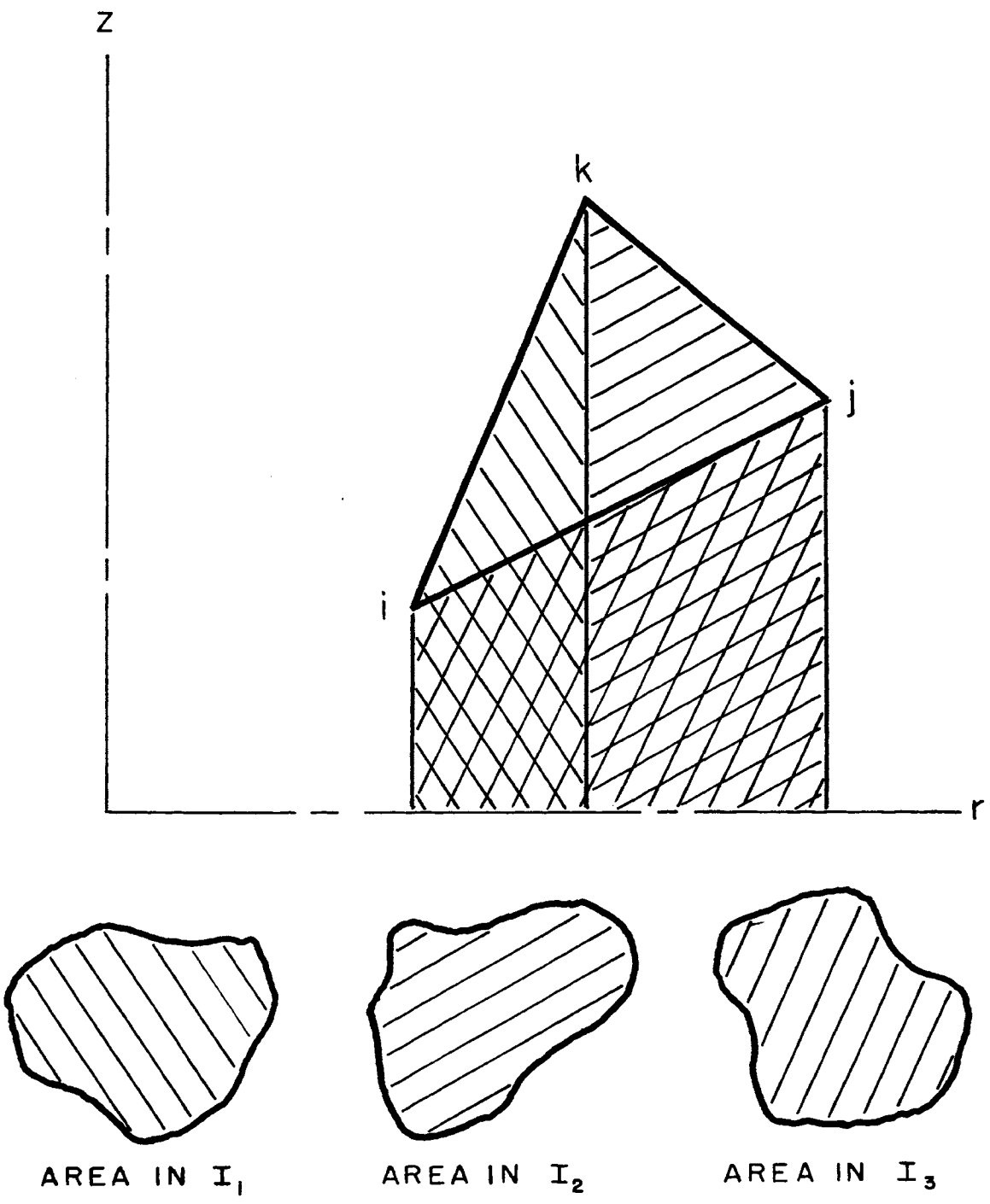

Figure 28. Triangular Element Sub-areas

all of the required functions and each is evaluated from the nodal coordinates of the elements.

Two circumstances arise which must be treated separately. They occur when the two radial coordinates are equal, and when one radial coordinate is zero when evaluating the area integral which contains the function r^{-1}. In the first circumstance, the values of η_1 and η_2 become infinite, but the value of the integral must be zero. Therefore, η_1 and η_2 are set to zero and further evaluation is omitted. In the second circumstance, it becomes necessary to evaluate a term containing a logarithm of zero. This term is evaluated using L'Hopital's rule and it is found that in the limit the term is equal to zero. Therefore, the term may be omitted.

APPENDIX D

LINE INTEGRALS

The line integral is required for various functional forms of r, z, and of s, the line itself. There are various combinations of r from the zero to the fourth power, z from the zero to the second power, and s from the zero to the first power.

To evaluate these integrals, both r and z are transformed to functions of s and the limits of s are calculated from the node coordinates. The integrals are evaluated in terms of the node coordinates along the boundary. The geometric relationships between the element surface boundaries and the coordinate systems are shown in Figure 2.

APPENDIX E

EXPERIMENTAL RESULTS

SPECIMEN NUMBER 1

Number of disks, 4

Width of disks, 0.125 inches

DIAMETER OF DISK (inches)	FLEXIBILITY X 10^4 (radians per inch-pound)
1.000	4.9038
0.875	4.8873
0.750	4.8869
0.625	4.8890
0.500*	5.0059

*Disks completely removed

Table II. Experimental Results, Specimen Number 1

SPECIMEN NUMBER 2

Number of disks, 4

Width of disks, 0.250 inches

DIAMETER OF DISK (inches)	FLEXIBILITY X 10^4 (radians per inch-pound)
1.500	4.7509
1.250	4.7402
1.000	4.7339
0.875	4.7349
0.750	4.7360
0.625	4.7785
0.500*	5.0093

*Disks completely removed

Table III. Experimental Results, Specimen Number 2

SPECIMEN NUMBER 3

Number of disks, 4

Width of disks, 0.500 inches

DIAMETER OF DISK (inches)	FLEXIBILITY X 10^4 (radians per inch-pound)
2.000	4.3394
1.500	4.3527
1.250	4.3532
1.000	4.3533
0.875	4.3617
0.750	4.4100
0.625	4.5281
0.500*	5.0045

*Disk completely removed

Table IV. Experimental Results, Specimen Number 3

SPECIMEN NUMBER 4

Number of disks, 3

Width of disks, 0.750 inches

DIAMETER OF DISK (inches)	FLEXIBILITY X 10^4 (radians per inch-pound)
2.000	4.2161
1.500	4.2025
1.250	4.2062
1.000	4.2230
0.875	4.2329
0.750	4.2959
0.625	4.4522
0.500*	4.9970

*Disk completely removed

Table V. Experimental Results, Specimen Number 4

SPECIMEN NUMBER 5

Number of disks, 3

Width of disks, 1.000 inches

DIAMETER OF DISK (inches)	FLEXIBILITY X 10^4 (radians per inch-pound)
2.000	3.9028
1.500	3.9012
1.250	3.9058
1.000	3.9306
0.875	3.9682
0.750	4.0617
0.625	4.2779
0.500*	5.0064

*Disk completely removed

Table VI. Experimental Results, Specimen Number 5

SPECIMEN NUMBER 6

Number of disks, 2

Width of disks, 1.500 inches

DIAMETER OF DISK (inches)	FLEXIBILITY X 10^4 (radians per inch-pound)
2.000	3.8503
1.500	3.8563
1.250	3.8577
1.000	3.8915
0.875	3.9311
0.750	4.0302
0.625	4.2642
0.500*	5.0004

*Disk completely removed

Table VII. Experimental Results, Specimen Number 6

SPECIMEN NUMBER 7

Number of disks, 2

Width of disks, 2.000 inches

DIAMETER OF DISK (inches)	FLEXIBILITY X 10^4 (radians per inch-pound)
2.000	3.4460
1.500	3.4607
1.250	3.4688
1.000	3.5152
0.875	3.5764
0.750	3.7102
0.625	4.0335
0.500*	5.0106

*Disk completely removed

Table VIII. Experimental Results, Specimen Number 7

SPECIMEN NUMBER 8

Number of disks, 2

Width of disks, 3.000 inches

DIAMETER OF DISK (inches)	FLEXIBILITY X 10^4 (radians per inch-pound)
2.000	2.5962
1.500	2.6171
1.250	2.6444
1.000	2.7170
0.875	2.8081
0.750	3.0261
0.625	3.5258
0.500*	4.9801

*Disk completely removed

Table IX. Experimental Results, Specimen Number 8

SPECIMEN NUMBER 9

Number of disks, 1

Width of disks, 5.000 inches

DIAMETER OF DISK (inches)	FLEXIBILITY X 10^4 (radians per inch-pound)
2.000	2.9737
1.500	2.9948
1.250	3.0163
1.000	3.0841
0.875	3.1707
0.750	3.3547
0.625	3.7783
0.500*	4.9863

*Disk completely removed

Table X. Experimental Results, Specimen Number 9

APPENDIX F

COMPUTER PROGRAM

The computer program written for this investigation is for the elastic stress analysis of a general axisymmetric solid. It provides for loads in four forms in each of the three directions. The loads may be due to (1) initial strains, (2) body forces, (3) distributed surface forces, and (4) concentrated loads. The displacements may be specified at any node, or along any boundary.

The input to the program allows several options which permit an abbreviated form of input by having intermediate data values calculated following a set pattern built into the program.

Due to the storage requirements for a complex structural problem, the program not only requires a large core storage but also some form of bulk storage. Computing time estimates for specific problems can be obtained by referring to the discussion in Chapter 3.

The input instructions and program listings are not included in this thesis. However, they are available from the author.

APPENDIX G

EQUIPMENT LIST

Load Cell - Daytronics Corp., Model 52A - 100, capacity 0 to 100 pounds

Transducer-amplifier - Daytronics Corp., Model 300D - V - 71

Voltmeter - Keithley Instrument, Guarded DC Voltmeter, Model 660 Å

Laser - Spectra-Physics, Model 130C

Power Meter - Spectra-Physics, 6328 Å, Power Meter

Dial Gage - Travel-Gage Corp.

BIBLIOGRAPHY

1. Fredrick, D., and Ching, T. S. Continuum Mechanics. Boston: Allyn and Bacon, 1965.

2. Sokolnikoff, I. S. Mathematical Theory of Elasticity. Providence: Brown University, 1941.

3. Timoshenko, S., and Goodier, J. H. Theory of Elasticity. 2nd edition. McGraw-Hill, 1951.

4. Willers, A. Die Torsion eines, Rotationionskorpers um seine Achse. Zeit. f. Math. u. Phys., 1907, 55, 225-263.

5. Sonntag, R. Zur Torsion von runden Wellen mit verandlichem Durchmesser. Zeit. F. angclew. Math. u, Mech., 1929, 9, 1-22.

6. Higgins, T. J. "Stress Analysis of Shafting Exemplified by Saint-Venant*s Torsion Problem", Exper. Stress Anal., III, 1, p. 94.

7. Freeman, N. J., and Leer, L. M. "Torsion of a Cylindrical Rod Welded to an Elastic Half Space", J. of Appl. Mech. - ASME, V 34, Series E, No. 3, p. 687, Sept., 1967.

8. Jacobsen, L. S. "Torsional-stress Concentrations in shafts of Circular Cross Section and Variable Diameter", Trans. Am. Soc. Mech. Eng., 47, 619-638, 1925.

9. Thum, A., and Bautz, W. "Zur Frage Der Formziffer", Zeit Verein Deut. Ing., 79, 1303-1306, 1935.

10. Wiegand, A. "Determenation of the Stress Concentration Factors of Fillets or Stepped Shafts Under Torsion (title trans)", Luftfahrt-Forihung, 20, 217-219, 1943. "Abstract", Automobile Engineer, 34, 1944.

11. Peterson, R. E. Stress Concentration Design Factors. New York: Wiley, 1953.

12. Frocht, M. M. Photoelasticity. Volume II. New York: Wiley, 1948.

13. Thom, A., and Orr,J. "The Solution of the Torsion Problem for Circular Shafts of Varying Radius", Pro. Roy. Soc., London: 1931, 131A, 30-37.

14. Southwell, R. V. Relaxation Methods in Engineering Science. Oxford University Press, 1940.

15. Turner, M. J., et al. "Stiffness and Deflection Analysis of Complex Structures", J. Aero. Sci., 23, p. 805-823, 1956.

16. Argyris, J. H. Recent Advances in Matrix Methods of Structural Analysis. New York: Pergamon Press, Oxford through MacMillan, 1964.

17. Zienkiewicz, O. C. The Finite Element Method in Structural and Continuum Mechanics. London: McGraw-Hill, 1967.

18. Jones, R. M., et al. SASS II, Finite Element Stress Analysis of Axisymmetric Solids With Orthotropic, Temperature-Dependent Material Properties. AD 679 983, 1968.

19. De Veubeke, B. F. "Displacement and Equilibrium Models in the Finite Element Method", Chapter 9 of Stress Analysis, ed. O. C. Zienkiewicz, and G. S. Holister, Wiley, 1965.

20. Argyris, J. H. "Triangular Elements With Linearly Varying Strain For the Matrix Displacement Method", J. Roy. aero. Soc. tech., 69, p. 711013, Oct. 1965.

21. Boresi, A. P. Elasticity in Engineering Mechanics. N.J.; Printice-Hall, 1965.

22. Fox, L. An Introduction to Numerical Linear Algebra. New York: Oxford University Press, 1965.

23. Fortran IV Language, IBM System / 360, IBM Systems Reference Library. File N. S. 360-25-GC28-6515-7, 1968.

24. "American Society of Testing Materials", Aluminium Alloy Specification, 7075.

25. "American Society of Testing Materials", Aluminium Heat Treatment Specifications, t-651.

26. Alcoa Aluminium Handbook. Aluminium Company of America, 1965

VITA

Richard King Riley, the son of Mr. and Mrs. Edward Riley, was born on July 4, 1936 in Marshalltown, Iowa.

He received his primary education in Fort Dodge, Iowa, and attended Sacred Heart High School in Fort Dodge, Iowa, graduating in May, 1954. He received an Associate of Arts degree in June, 1957 from Fort Dodge Junior College, Fort Dodge, Iowa. At the State University of Iowa, Iowa City, Iowa, he was awarded a Bachelor of Science degree in Mechanical Engineering in June, 1961, and a Master of Science degree in Mechanical Engineering in January, 1965.

In September, 1966, he enrolled in Graduate School at the University of Missouri - Rolla, and also received an appointment as Instructor in the Department of Mechanical and Aerospace Engineering, which he has held since that time.

He was married to Miss Donna Lee Mossman in June, 1961 and they now have two children.